Winter 3-18-2017

# UV-Vis and Fluorescence Studies of Zinc Enzyme Active Site Mimics and Their Binding of Inhibitor Compounds

Aeshah Hussain Niyazi
*DePaul University*, ayshanyazi@yahoo.com

# UV-Vis and Fluorescence Studies of Zinc Enzyme Active Site Mimics and Their Binding of Inhibitor Compounds

A Thesis

Submitted to the Faculty of

DePaul University

By

Aeshah Hussain Niyazi

In Partial Fulfillment of the

Requirements for the Degree

Of

Master of Science

November 2016

DePaul University

Chicago, Illinois

This work is dedicated to my beloved parents.

Table of Contents

## Table of Figures, Tables and Schemes

Abstract

This research aimed to synthesize and characterize $Zn^{2+}$-ligand complexes that have the same zinc coordination environment as in *histone deacetylase* (HDAC) and other important zinc-dependent enzymes. Mimicking the structural and the functional properties of $Zn^{2+}$-enzymes will allow us to understand the binding reactivity between $Zn^{2+}$ and small molecule enzyme inhibitors. The new understanding will help to develop new approaches to target disease states such as cancer. A variety of $Zn^{2+}$ binary complexes have been synthesized and their interactions with inhibitors such as suberanilohydroxamic acid (SAHA) and 8-Hydroxyquinoline (8HQ) have been studied using $^1$H NMR, UV-Vis, and fluorescence spectroscopies. Attempts were made to mimic the structure of $Zn^{2+}$-metalloenzyme active sites by exploring several different supporting ligands to model enzyme active sites. We endeavored to mimic an "$O_2N$" ligand set of HDAC by using reported $Zn^{2+}$-complexes ligated by Bis(phenolato)amine (**$H_2$L1**), Bis(2-picolyl) amine (BPA, **L2**), hydrotris(3-phenyl-5-methylpyrazol-1-yl) ($Tp^{Ph,Me}$, **L3**), and a similar neutral ligand (**L4**). The binding constants of the ligands with zinc were estimated using UV-Vis studies and calculations based on equilibrium expressions. This data was compared with previously reported data using other methods such as potentiometry and isothermal titration calorimetry.

Once the zinc-ligand complexes were obtained, they were examined for mimicking zinc active sites. Attempts were made to study the interaction of inhibitors with the zinc center using $^1$H NMR, UV-Vis, and fluorescence spectroscopies. In addition, the functional properties of the mimicked structure were explored by attempting to cleave the amide group of a model substrate for *HDAC*, N-acetylbenzylamine. Although the $Zn^{2+}$ species were not active, $Al^{3+}$ was observed to cleave the amide group at high temperature after extended periods of time. The zinc-ligand

structures were also examined using computational methods to support the experimental data. The results of this work are valuable complementary data to previously reported ITC data and the known biological systems.

## Chapter 1. Introduction

Zinc plays a variety of critical roles in biology. An average adult human body contains 3 grams of zinc, present in all body muscle tissue, and in higher concentrations in various organs such as prostate and eye tissue (retina and choroids).[1] Zinc is the second most abundant transition metal in our bodies after iron.[2] In medicine, zinc is important because it has been shown to help prevent the effects of infectious diseases such as malaria and pneumonia, and to shorten the length of common cold in adults.[1] At a molecular biology level, zinc is an essential component in approximately 300 enzymes within six main classes: oxidoreductases, transferases, hydrolases, lyases, and isomerases.[3,4] These zinc-dependent enzymes play a significant role in the progression of human diseases. For example, zinc is indispensable for the effective growth and development of cancer cells. Thus, zinc-containing enzymes are potential targets for the treatment of cancer in humans.

In metal-based enzymes, the binding between the metal in the active site and various ligands such as substrates or inhibitors depends on many factors. It is often useful to invoke the "Hard-soft acid-base" (HSAB) theory, in which strong bonding occurs when a hard acid and hard base or a soft acid and soft base interact. Zinc is a "borderline" metal, which means the interactions between the Zn and both hard and soft donor atoms in the ligand are equally favorable.[4] Likewise, the divalent $d^{10}$ $Zn^{2+}$ ion is exceptionally stable with respect to oxidation and reduction under biological conditions, and so does not participate in redox reactions, as compared to the redox-active biological metals Mn, Fe, and Cu. Zinc often plays a role of activating reagents via donor-acceptor interactions. One classic example of an enzyme with a zinc atom in its active site is *carbonic anhydrase* (CA). The *carbonic anhydrase* enzymes are

oldest known class of Zn metalloenzymes, which was discovered in 1940 by Brinkman *et al* (Figure. 1.1).[5]

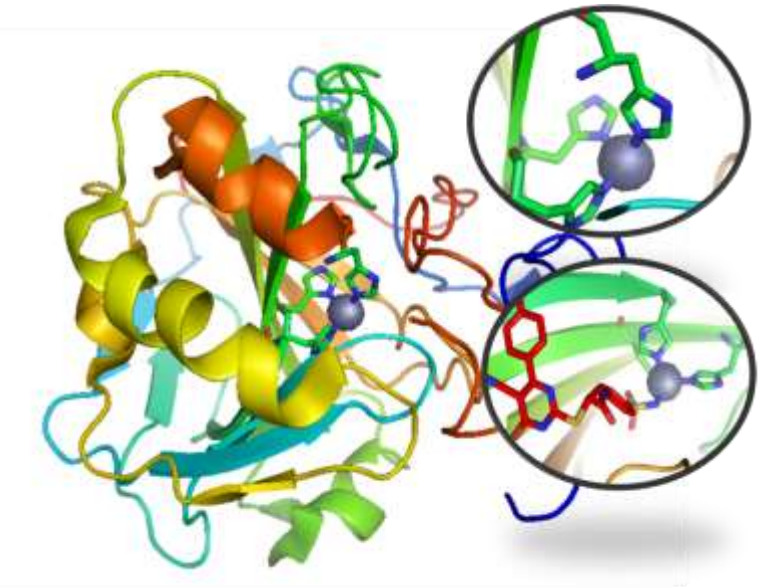

**Figure 1. 1. Carbonic anhydrase II (CA). Image from the RCSB PDB of PDB ID 5J8Z, and generated by PyMol**. The upper Figure shows the binding between the Zn and three histidines, and the second figure shows a carbonic anhydrase inhibitor binding with $Zn^{2+}$.[1]

The CA enzyme contain four ligands binding with $Zn^{2+}$ in the resting state of the catalyst, three Histidine residues (His) and a nucleophilic, activated hydroxide molecule occupies the fourth coordination site, providing a distorted tertahedral geometry.[6] Human CA plays an important role in regulation the pH and fluid balance in different parts of human body.[7] It catalyzes the reversible hydration of bicarbonate ion to form carbon dioxide, as per the following reaction:

$$CO_2 + H_2O \rightleftharpoons HCO^-_3 + H^+$$

The inhibition of human CA can have harmful effects on the body in the form of acidosis as blood pH homeostasis is disrupted.[8] The tetrahedral coordination in Zn and the surrounding

amino acids enhance both the Lewis acidity of the zinc center and the Brønsted acidity of a coordinated water molecule.[6] Ligand field stabilization effects do not influence zinc complexes due to the $d^{10}$ configuration of $Zn^{2+}$, and so coordination number and geometry are quite flexible and are only affected by ligand size and charge. Hydrolytic Zn-enzymes are capable of hydrolyzing a variety of strong bonds, such as hydrating $CO_2$ in *carbonic anhydrase*, cleaving amide bonds (RC(O)-NHR′), or cleaving a phosphate bond.[1]

Amide bonds are very stable in biology, but they can be hydrolyzed by Zn-dependent enzymes. Each particular amide hydrolysis enzyme targets a specific type of amide bonds. For example, *carboxypeptidase* hydrolyzes the C-terminus in a peptide residue, *collagenase* hydrolyzes collagen, *dipeptidase* hydrolyzes dipeptides and *Histone Deacetylase* (HDAC) hydrolyzes an acetamide group of a lysine residue on a Histone protein (Figure 1.2).[9] One approach to the development of cancer drugs is targeting the enzymes that allow the uncontrolled replication of cancer cells. *Histone deacetylase* enzymes (HDAC) are one class of these targeted enzymes. Inhibiting these enzymes prevents the remove of the acetyl groups on N-acetyl lysine residues in histone proteins.[10] Deacetylation plays an important role in many gene regulations, especially regulation of gene transcription. Histone components are present in the core of chromatin in DNA, and they control transcription and play an essential role in gene regulation.

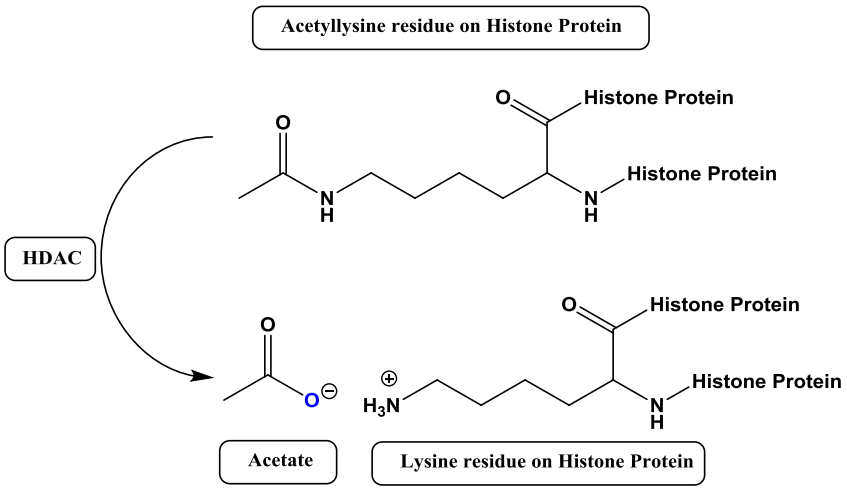


**Figure 1.2. The deacetylation by HDACs of the acetyl group from lysine in the presence of water, releasing an acetate molecule.**

The nucleosome is the fundamental unit of chromatin and it is composed of an octamer of the four core histones (H3, H4, H2A, H2B) around which 147 base pairs of DNA are wrapped (Figure1.3).[11] The histone is important for establishing different ionic interactions between nucleosomes in chromatin. Therefore, chromatin can adopt different structural conformation depending on modifications that occur in the histone tails, specifically H-3 and H-4, which are targeted for various post-translational modifications such as acetylation, N-methylation, or phosphorylation.[12] The mechanism of gene-transcription includes neutralizing the positive charge of histone lysine residues in order to result in more relaxed chromatin. Deacetylation of histone lysine residues increases ionic interactions between positively charged histones and negatively charged DNA, resulting in condensed chromatin and limiting gene transcription.

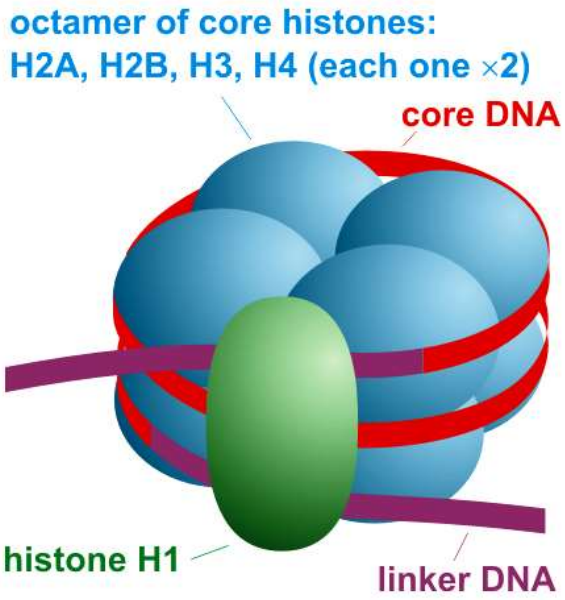


**Figure 1.3. The nucleosome is the basic unit of chromatin and it consists of DNA wrapped around a histone octamer.[2]**

*Histone deacetylases* comprise a family of 18 enzymes, which are grouped into classes I–IV based on their homology to their respective yeast orthologues. Classes I, II and IV contain 11 family members, which are referred to as classical HDACs; the other 7 members are in class III which are called sirtuins. Studies have shown that the classical HDACs are promising targets for anti-cancer drugs.[12] Inhibition of HDACs can be used as a therapeutic approach to prevent deacetylation thus prevent cancer cells from replicating genes, and eventually killing them. Classes (I\II) show effective targets toward inhibiting cancer cells. In these two classes, a wide range of HDAC enzymes share the same structural characterization, which comprise of a zinc active site at the bottom of a tubular pocket.

In HDAC, zinc is coordinated by two His residues and an aspartate residue as well as a water/hydroxide. It has been well recognized that certain *histone deacetylase* enzymes inhibitors

(HDACI) are promising cancer therapeutic agents.[10,12,13] These inhibitors act by binding the HDAC, thus modifying gene expression to restore the normal differentiation or kill the programs of transformed cells. Several HDACIs have been isolated as natural or synthesized products. HDACs have been classified into 3 classes (I\II) NAD- dependent and class (III) (HDAC) Histone deacetylase enzyme. One example of a good HDAC inhibitor is suberanilohydroxamic acid (SAHA, also known as Vorinostat), which contains a zinc-binding group connected to an aliphatic chain and a capping group (Fig. 1.4).[14,15] These three general components can also been found in several other HDACIs.

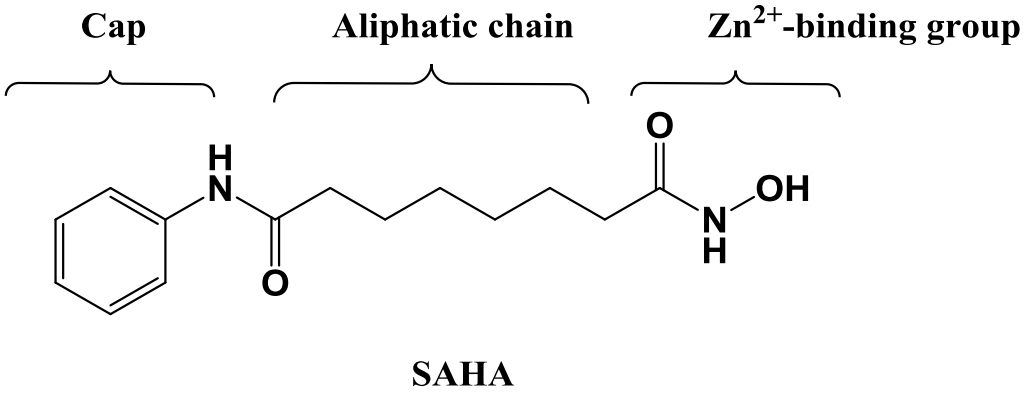


**Figure 1.4. The Structure of Vorinostat (SAHA) and the general structure of HDACIs.** Three general regions that many HDACIs are comprised of: a cap, an aliphatic chain, and a zinc-binding group.

Vorinostat (SAHA) was the first drug approved by the FDA as a treatment for cutaneous T-cell lymphoma and is an effective HDACI.[13] In addition to targeting cancer cells, HDACIs including SAHA have been identified as potential treatments of metabolic diseases, inflammatory diseases, neurodegenerative disorders, and cardiovascular disease. Another inhibitor used in this study was 8-Hydroxyquinoline (8HQ) (Figure 1.5). 8HQ is a

monohydroxyquinoline compound, which are found in plants and have a variety of known synthetic variants. It is a well-known strong chelator of metal ions with the ability to bind Zinc. It is worth noting that 8HQ derivatives also have pharmacological application to a wide range of diseases, such as HIV, breast cancer, prostate cancer, and fungal infections.[9]

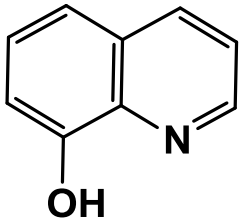


**Figure 1.5. The 8-Hydroxyquinoline (8HQ) structure.**

Although some progress has been made to understand drug-zinc interactions, a better understanding of the specific interactions between the zinc active site and the drug molecules is needed in order to design better drugs to treat cancers and other disorders. However, it is very difficult to work with the native enzymes, as they are time-consuming and challenging to produce in large amounts. In addition, the large size of enzymes makes spectroscopic techniques that target the active site difficult to perform and interpret. Instead, we chose to attempt to mimic the active site of the zinc enzymes by synthesizing small zinc-containing molecules that are models of the active site structures. Mimicking the structural and the functional properties of Zn enzymes will allow us to understand the binding reactivity between $Zn^{2+}$ and its inhibitors and that new understanding will lead us to develop new techniques to deliver inhibitors or drugs to cancer cells. A variety of zinc complexes and their interactions with inhibitors such as SAHA and 8HQ have been studied.[1-4,6,10-13] Previously, the interactions between zinc and various

ligands and inhibitors were examined in solution using isothermal titration calorimetry (ITC) in Dr. Jin's lab in collaboration with Dr. Karver and Dr. Grice.[16]

In this work, several attempts were made to mimic the structure of $Zn^{2+}$ metalloenzyme active sites shown in Figure 1.6 using complementary techniques to ITC to obtain more information. We explored different supporting ligands to examine the active site structures including methylamino-*N,N*-bis(2-methylene-4.6-di-*tert*-butylphenolato) (**$H_2$L1**), bis(2-picolyl) amine (BPA, **L2**), hydrotris(3-phenyl-5-methylpyrazol-1-yl) ($Tp^{Ph,Me}$, **L3**), and a similar neutral ligand (**L4**) (Figure 1.6). in previous work, complexes of BPA and $Tp^{Ph,Me}$ have been examined for mimicking zinc active sites.[13,16] In addition, the x-ray structures of Zn(**L2**) and Zn(**L3**) complexes are known.[13,16,17] The zinc complexes of these ligands were synthesized and then used in further studies (Figure 1.7). Given the small size of these complexes relative to the actual enzyme, we were able to study the interaction of enzyme inhibitors with the zinc center and also to characterize the functional properties of the mimicked structure by attempting to cleave a model amide group. More importantly, we studied the interaction of $Zn^{2+}$-ligands towards inhibitors of *histone deacetylase*, such as Vorinostat (SAHA) and 8-hydroxyquinoline (8HQ). The results of this study are reported in the following chapters. Chapter 2 reports the experimental details of the studies. Chapter 3 reported the studies of the interaction between $Zn^{2+}$ and the ligands in Figure 1.6, and the functionality of these complexes (Figure 1.7). Chapter 3 also studies of the interaction of inhibitors with the $Zn^{2+}$-ligand binary complexes that had been previously identified as potential *HDAC* structural mimetics. Lastly, chapter 4 reports the interaction between $Zn^{2+}$ and ligands and between $Zn^{2+}$ and inhibitors using UV-Vis and fluorescence spectroscopies.

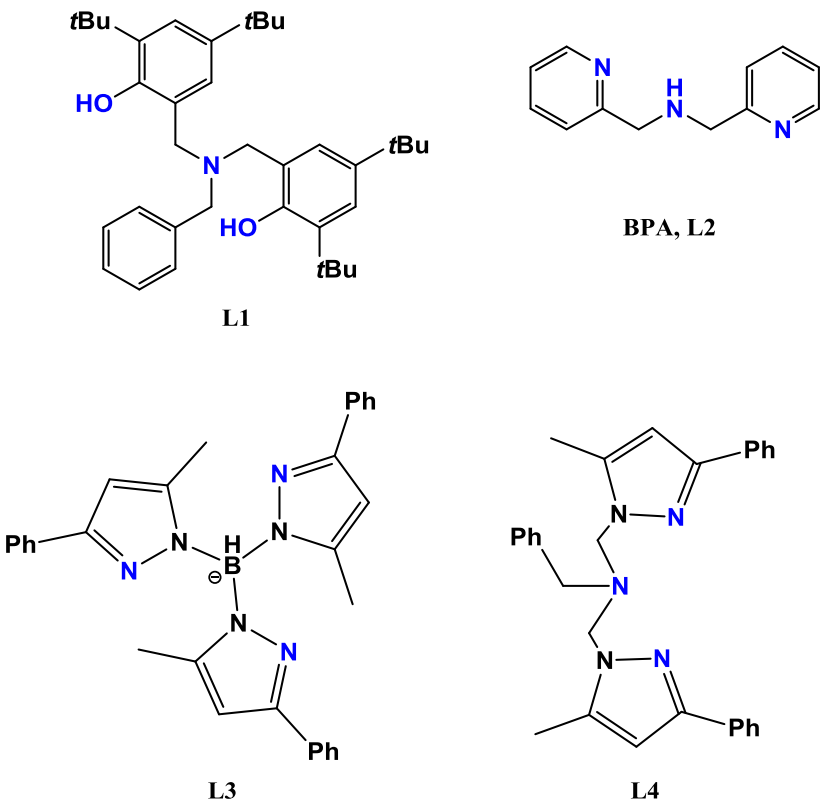


**Figure 1. 6. Ligands explored in this work.** On the top right is a benzyl-stubstituted bis(phenolato)amine (**$H_2$L1**), **L2** is bis(2-picolyl)amine (BPA), **L3** is hydrotris(3-phenyl-5-methylpyrazol-1-yl) ($Tp^{Ph,Me}$), and **L4**. The atoms that can bind to metals are highlighted in blue.

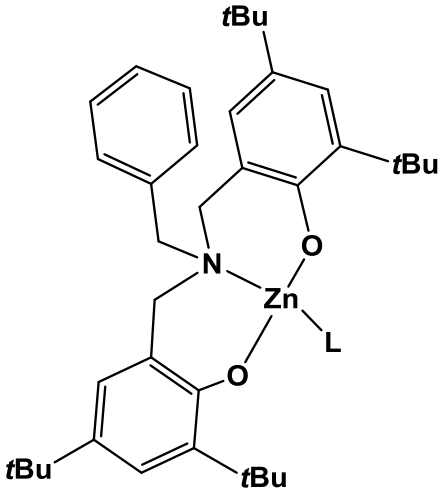


Zn(L1)

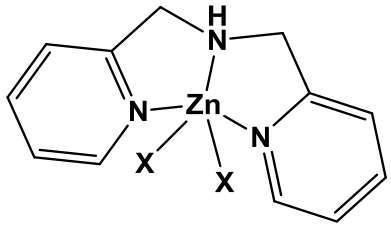


$Zn(L2)X_2$

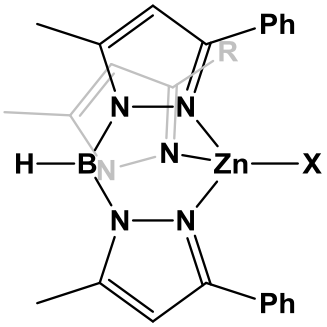


Zn(L3)X

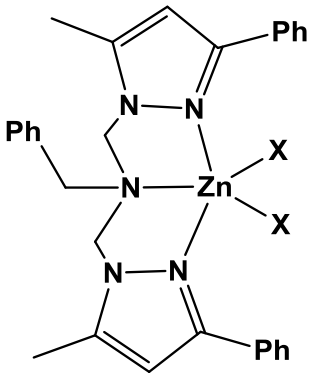


$Zn(L4)X_2$

**Figure 1.7. Zinc Complexes of Ligands L1, L2, L3 and L4**. The image shows the general expected bonding patterns for these complexes. L and X refer to generic neutral and anionic ligands, respectively.

## Chapter 2. Experimental methods

### 2.1. General considerations

All reactions and processes were carried out on the benchtop in the presence of air unless otherwise noted. $Zn[N(TMS)_2]_2$ was purchased from Sigma Aldrich, and BPA ( > 98.5%) was purchased from TCI. All other reagents and solvents were purchased from commercial suppliers and used as supplied. All NMR spectra were collected using a Bruker Avance 300 MHz NMR spectrometer at 298 K. $^1$H NMR spectra were referenced against residual solvent peaks and reported downfield of tetramethylsilane ($\delta$ = 0 ppm). UV–Visible (UV–Vis) spectra were obtained with a Varian Cary 100 UV–Vis spectrometer. Infrared (IR) spectra were collected on an ABB FTLA2000 IR spectrometer equipped with a PIKE Technologies MIRacle diamond ATR (attenuated total reflectance) anvil. Fluorescence spectra were obtained with a Varian Cary Fluorescence spectrophotometer.

### 2.2. Preparation of the Ligands, Zn-ligands, and reactions of (ZnL) with inhibitors

#### 2.2.1. Synthesis of **$H_2$L1**

The methylamino-*N,N*-bis(2-methylene-4.6-di-*tert*-butylphenolato) (**$H_2$L1**) was synthesized in two steps based on a modification of the procedure by Silvernail C. and co-workers. A solution of methylamine (7.5 ml, 0.2 mol) was added dropwise at 0 °C to a stirring solution of paraformaldehyde (5.2 g, 0.2 mol) and KOH (0.01 g, 0.2 mol) in 25 ml of ethanol. After the mixture was allowed to warm to room temperature, a second solution of 2,4-di-*tert*-butylphenol (35.5 g, 0.2 mol) in 25 ml ethanol was added to the first mixture in one portion. The reaction was heated to reflux for 24 h. After allowing the reaction to cool, the solvent was removed under vacuum, and the product was rinsed with 20 mL of ethanol. The final product was a white solid (2.11 g, 3.4%). NMR data matched literature values.[3]

2.2.2. Synthesis of $[Zn(\mathbf{L1})]_2$

$[Zn(\mathbf{L1})]_2$ was prepared by adding $Zn[N(TMS)_2]_2$ (0.3 ml, 5.7 mmol, TMS = trimethylsilyl) to a stirring solution of $\mathbf{H_2L1}$ (70 mg, 5.7 mmol) in 5 ml toluene. The green mixture was stirred at room temperature for 16 h. A light green powder (0.03 mg, 43%) was obtained after washing the product with 5 ml pentane. $^1$H NMR (300 MHz, $CD_2Cl_2$): δ = 5.32 (s, 2H), 7.30 (s, 2H, PhH), 7.09 (s, 2H, PhH), 7.02 (s, 2H, PhH), 6.70 (s, 2H, PhH), 4.98 (d, J) 13 Hz, 2H, $CH_2$), 3.90 (d, J) 13 Hz, 2H, $CH_2$), 3.40 (d, J) 13 Hz, 2H, $CH_2$), 2.57 (d, J ) 13 Hz, 2H, $CH_2$), 1.39 (s, 18H, t Bu), 1.29 (s, 18H, t Bu), 1.20 (s, 18H, t Bu), 1.18 (s, 18H, t Bu).

2.2.3. Reaction of $[Zn(\mathbf{L1})]_2$ with suberanilohydroxamic acid (SAHA)

$[Zn(\mathbf{L1})]_2$ (0.3 g, 0.02 mmol) and SAHA (6.5 g, 0.02 mol) were dissolved in 10 ml acetonitrile. The reaction was stirred for 24 h in a 60 °C oil bath, and then the solvent was removed under vacuum. Crystallization was attempted using vapor diffusion by dissolving the product in methanol and placing the vial in a larger vial filled with pentane. The product did not crystallize, therefore the solvent was removed under vaccum and the mass of the solid was obtained (44.1 mg, 86.5%). IR and $^1$H NMR spectra are shown in chapter 4.

2.2.4. Reaction of $[Zn(\mathbf{L1})]_2$ with 8-hydroxyquinoline (8HQ)

$[Zn(\mathbf{L1})]_2$ (50 mg, 0.04 mmol) and 8HQ (5.9 mg, 0.04 mmol) were dissolved in 5 ml acetonitrile. As soon as 8HQ was added, the color of the mixture turned to yellow. The reaction was stirred for 24 h in a 60 °C oil bath. The product was then dried using a rotary evaporator, resulting in a yellow power with a 0.05 g yield (85.7%). $^1$H NMR spectra are shown in chapter 4.

2.2.5. Synthesis of Zn(**L2**)$Cl_2$

A sample of commercially purchased bis(2-picolyl)amine (BPA, **L2**) (0.25 ml, 0.1 mmol) was added to stirring solution of (17 mg, 0.1 mmol) of zinc dichloride and 5 ml methanol. The reaction as heated at 60 $^{\circ}$C for 24 h. The product was filtered and dried. Spectral data matched literature values.[16]

2.2.6. Reaction of Zn(**L2**)$Cl_2$ with 8HQ

A sample of Zn(BPA)$Cl_2$ (0.8 mg, 3.4 mmol) and 0.5 mg (3.4 mmol) of 8HQ were dissolved in 5 ml acetonitrile (ACN). The reaction was stirred in 60 $^{\circ}$C oil bath for 48 h. the $^{1}$H NMR spectra are shown in chapter 4.

2.2.7. Previous syntheses of Zn(**L3**)OH, Zn(**L3**)(8HQ), and **L4**

Zn(**L3**)OH and Zn(**L3**)(8HQ) were previously prepared in Dr. Grice's lab by other researchers.[13] The ligand **L4** was prepared by Mark Gudger in the Grice lab and characterized by $^{1}$H and $^{13}$C{$^{1}$H} NMR as well as X-ray crystallography and elemental analysis (unreported data).

2.3. Other experimental details

2.3.1. Attempted synthesis of a benzylated version of **$H_2$L1**

An attempt was made to synthesize a benzylated version of **$H_2$L1**, benzylamino-*N,N*-bis(2-methylene-4.6-di-*tert*-butylphenolato). A solution of benzylamine (9.45 ml, 0.1 mol) was added dropwise at 0 ˚C to a stirring solution of paraformaldehyde (5.2 g, 0.2 mol) and KOH (0.077 g, 1.2 mmol) in 25 ml of ethanol. After the mixture was warmed to room temperature, a second solution of 2,4-ditertbutylphenol (35.5 g, 0.2 mol) in 25 ml ethanol was added to the first mixture in one portion and the reaction was heated to reflux for 24 h. After allowing the reaction to cool, the solvent was removed under vacuum, and the product was rinsed with 20 mL of

ethanol. The final product was a white solid (18.8 g, 89.9%). $^1$H NMR (300 MHz, $CDCl_3$): δ = 7.20 (m, 5 H, Ar), 7.07 (d, $J_{HH}$ = 2.80 Hz, 1H, Ar), 6.67 (d, $J_{HH}$ = 2.21 Hz, 1 H, Ar), 4.71 (s, 2 H, $NCH_2O$), 3.90 (s, 9 H, $ArCH_2N$), 3.80 (s,2 H, $CH_2Ph$), 1.70 ((s, 2, $C(CH_3)_3$), 1.30 ((s, 2, $C(CH_3)_3$) ppm.[18] When comparing these spectra with the spectra for **$H_2$L1**, it showed different signals than would be expected for the desired product. Therefore, the final product is not of the fomula $H_2L$, but rather using benzylamine as a starting material yielded a benzoxazine product (Scheme 2.3.1).

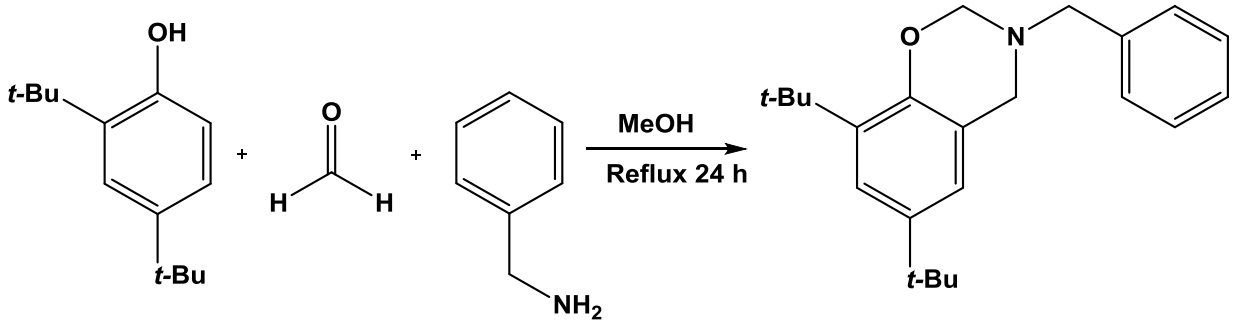


**Scheme 2.1. Benzoxazine synthesis**. This reaction occurred during instead of the desired ONO ligand (a derivative of **$H_2$L1)**.

2.3.2. Alternative synthesis of [Zn(**L1**)]$_2$

An alternative approach was performed by using a different Zn-containing species as a starting material. $Zn(OAc)_2 \cdot 2H_2O$ (21 mg, 0.1 mmol) was added to a stirring solution of (70 mg, 0.1 mmol) (**$H_2$L1**) and 5 mL toluene. The reaction was stirred for 14 h at ambient temperature. Then, the solvent was evaporated to dryness on rotary vaporator and a light green solid was formed. $^1$H NMR (300 MHz, CDCl3): 7.24 (s, 2H, PhH), 7.23 (s, 2H, PhH), 7.18 (s, 2H, PhH), 7.16 (s, 2H, PhH), 4.86 (s, 2H, $CH_2$), 4.63 (s, 2H, $CH_2$), 3.64 (s, 2H, $H_2O$), 3.45 (s, 2H,$CH_2$), 2.33 (d,*J* 13 Hz, 2H, CH2), 2.11 (s, 3H, $CH_3$), 12.03 (s,18H, *t*Bu), 1.40 (s, 18H, *t*Bu), 1.28 (s, 18H, *t*Bu), 1.25 (s, 18H, *t*Bu).

2.3.3. Reaction of $[Zn(\mathbf{L1})]_2$ with SAHA and base

Suberanilohydroxamic acid (10.8 mg, 0.4 mmol), a sample of KOH (2.3 mg, 0.04 mmol) and 18-crown-6 (10 mg, 0.03 mmol) were added to 7 ml methanol. The reaction was allowed to stir until complete dissolution. Next, 50 mg (0.04 mmol) of $[Zn(\mathbf{L1})]_2$ was added to the reaction, then it was allowed to stir at room temperature for 24 h. The solution was evaporated to dryness on a rotary vaporator, and a white solid was recrystallized from tetrahydrofuran (2 ml). However, the solid did not precipitate and therefore the solvent was removed. $^1$H NMR spectra was taken, and showed *tert*-butyl signals at the shifts of δ = 1.39 (s, 18H, *t*Bu), 1.29 (s, 18H, *t*Bu), 1.20 (s, 18H, *t*Bu), 1.18 (s, 18H, *t*Bu).

2.3.4. Attempted deprotonation of SAHA

Suberanilohydroxamic acid (SAHA) (0.2 g, 0.7 mmol) was added to 5 ml methanol. In the same mixture, 18-crown-6 (0.2 g, 0.7 mmol) and KOH (0.04 g, 0.7 mmol) were added. The reaction was allowed to stir at room temperature for 3 h. the solution was evaporated to dryness on a rotary vaporator. The resulting compound was a clear oil. $^1$H NMR (300 MHz, $CDCl_3$) δ = 7.72 (*d*, 2H), 7.03 (*t*, 1H), 2.37 (*t*, 2H), 2.19 (*t*, 2H), 2.00 (*s*, 1H), 1.87 (*d*, 1H), 1.74 (*t*, 2H), 1.64 (*t*, 2H), 1.40 (*s*, 2H). THF (2 ml) was added; however, the solid only partially dissolved. Therefore, the mixture was separated by glass wool into a solid and a solution. The solid was recrystallized in THF by allowing pentane to vapor diffuse into the solution. However, a yellow semi-crystalline viscous material was produced instead of crystals. The solution was evaporated to dryness and the residue was dissolved in methanol. Pentane was allowed to vapor diffuse into methanol. Small particles were observed and the product was washing four times with THF to yield a white solid (1.6 mg, 0.4%). The characteristic IR peaks for (O-H) and (N-H) in SAHA are: 3286, 3251 and 3137 $cm^{-1}$. As in this range, it was hard to differentiate the (O-H) bands

from the (N-H) bands. In comparison, the IR spectra for deprotonated SAHA shows one band at 3306 $cm^{-1}$. The lack of the broad band in the same region indicates that SAHA might be protonated. T $^1$H NMR showed that this material matched SAHA, and the IR spectra displayed a broad band for (O-H) that differed from SAHA's IR spectra and the deprotonated IR spectra. Together, this indicates that deprotonation did not occur.

2.3.5. Reaction of $[Zn(\mathbf{L1})]_2$ with 8HQ

A sample (31 mg, 0.05 mmol) of $[Zn(\mathbf{L1})]_2$ was added to 5 ml chloroform-*d*. In the same solution, 8.3 mg (0.05 mmol) of 8HQ, 0.31 mg (0.05 mmol) of KOH, and 15 mg (0.05 mmol) of 18-crown-6 were added. The reaction stirred for 24 h in ambient temperature. The solution was evaporated to dryness.

2.4. Attempted hydrolysis of amide bonds

Several Zn-ligand complexes were examined as catalysts to hydrolyze a secondary amide bond in a small molecule substrate. The general procedure was as follows: 1 equivalent of Zn-ligand species and one equivalent of N-benzylacetamide (the substrate) were dissolved in dimethyl sulfoxide-$d_6$ (DMSO-$d_6$) and water (1:1 solution). The mixture was heated and stirred in an oil bath at 100 °C for a long period of time (several days). $^1$H NMR spectra were collected for each reaction and are shown in Chapter 3. The$^1$H NMR spectra of benzylamine and N-phenylacetamide were taken to compare with the spectra of the reactions of each ZnL. $^1$H NMR (300 MHz, DMSO) for benzylamine: δ =7.21-7.37 (s, 5 H, Ph), 3.87 (s, 2H, $CH_2$) and 1.41 (s, 2H, $NH_2$). $^1$H NMR for N-phenylacetamide (300 MHz, DMSO) δ = 7.31 (s, H, NH), 7.29 (s, 2H, Ph), 7.25 (s, 2H, Ph), 7.23(s, H, Ph), 4.25-4.23 (d, 2H, $CH_2$), 1.86 (s, 3H, $CH_3$).

2.5. UV-Vis analysis of the interaction between $Zn^{2+}$, Ligands and inhibitors

Different concentrations of Zn-ligand complexes were dissolved in 5 ml acetonitrile (ACN). We attempted this process for all ZnL species reported in this thesis. The Varian UV Scan software was used to collect the data. Quartz cuvettes were used in order to avoid dissolving plastic cuvettes with organic solvents. In addition, different concentrations of Zn(**L2**)$Cl_2$ were dissolved in 5 ml buffer solution (50 mM NEM, 0.15 M NaCl, pH 6.8). After taking the spectra of Zn-ligand complexes, a fixed amount of $ZnCl_2$ (7 mg) was added to the measured solution of Zn-ligand. Then, the spectra of (ZnL) and the additional $ZnCl_2$ was taken. Spectra are shown in chapter 4 section 4.1.

2.6. Fluorescence analysis of the interaction between Zn, ligands and inhibitors

The maximum fluorescence emission wavelengths of Zn-ligands and inhibitors were collected using excitation wavelengths at 240 nm, 260 nm and 310 nm. We used these wavelengths to determine the emission spectra of each Zn-ligand-inhibitors species. The software used was Cary Eclipse Scan. The general procedure involved using a small amount of Zn-ligand (*ca.* 1 mg) and inhibitor dissolved in 5 ml acetonitrile. Spectra are shown in chapter 4.

## Chapter 3. Synthesis of zinc species and their interaction with inhibitors, and assessment of hydrolysis activity

The focus of this project was to form mimetic complexes of the HDAC active site and study their interactions with different HDAC inhibitors. The design of the Zn-ligand complexes must obey certain requirements to be qualified as mimicking zinc enzymes active sites. Previous ITC studies of the interaction of $Zn^{2+}$ with several ligands indicate that for a successful mimetic, the ligand must strongly chelate to $Zn^{2+}$, form a complex with a zinc-to-ligand ratio of 1:1, and still have open coordination sites for the inhibitor to interact.[16] $Zn^{2+}$ coordination complexes can exist in solution with tetrahedral, trigonal bipyramidal, or octahedral geometries. The tetrahedral and trigonal bipyramidal geometries are particularly preferred by $Zn^{2+}$, and provide only four or five total coordination sites, respectively. Therefore, using tetradentate or pentadentate ligands to form the zinc:ligand complex leads to insufficient coordination sites left on $Zn^{2+}$ for the inhibitor binding.[16] Both inhibitors used in this study are bidentate chelating ligands, which makes them good inhibitors to bind metals in enzyme active sites because their coordination will be stabilized by the chelate effect. In this chapter the synthesis of zinc enzyme active site mimics are reported along with their interaction with enzyme inhibitors, as studied by NMR spectroscopy. The ability of the zinc complexes to act as functional mimics of HDAC is also explored. Finally, computational calculations were performed to optimized Zn(**L1**) and Zn(**L1**)(AHA) structures.

### 3.1. Ligands with O, N, O coordination framework

#### 3.1.1. Synthesis of $\mathbf{H_2L1}$ and its zinc binary complex

Given that the coordination geometry of the HDAC active site contains two aspartates and a histidine residue, we sought to mimic this with a tridentate ligand with one nitrogen and two oxygen donors. Methylamino-*N,N*-bis(2-methylene-4,6-di-*tert*-butylphenol ($\mathbf{H_2L1}$) is a

tridentate ligand that can bind to transition metal ions such as $Zn^{2+}$ (Figure 1.6). The $[Zn(\mathbf{L1})]_2$ complex was studied by Silvernail C. M. and co-workers using $^{1}H$ NMR, $^{13}C$ NMR spectroscopy and X-ray crystallography.[3] $\mathbf{H_2L1}$ was prepared by a condensation of methylamine, paraformaldehyde and *tert*-butylphenol in refluxing methanol. Then, the addition of $Zn[N(TMS)_2]_2$ resulted in a dimeric complex, $[Zn(\mathbf{L1})]_2$. In the solid state, the complex possesses a dinuclear structure with each $Zn^{2+}$ ion coordinating two oxygens and one nitrogen of each *bis*-phenolate amine and coordinating to an oxygen of a second molecule of the Zn(**L1**) monomer. However, it has been reported that in solution such as tetrahydrofuran-$d_8$, this dimeric compound is in equilibrium with a monomeric solvent-bound structure (Scheme 3.2). In addition to following the reported synthesis, we found that the specialized reagent $Zn[N(TMS)_2]_2$ was not necessary for synthesis of $[Zn(\mathbf{L1})]_2$. The cheaper and less sensitive salt $Zn(OAc)_2{\cdot}2H_2O$ was equally effective in reaction with $\mathbf{H_2L1}$.

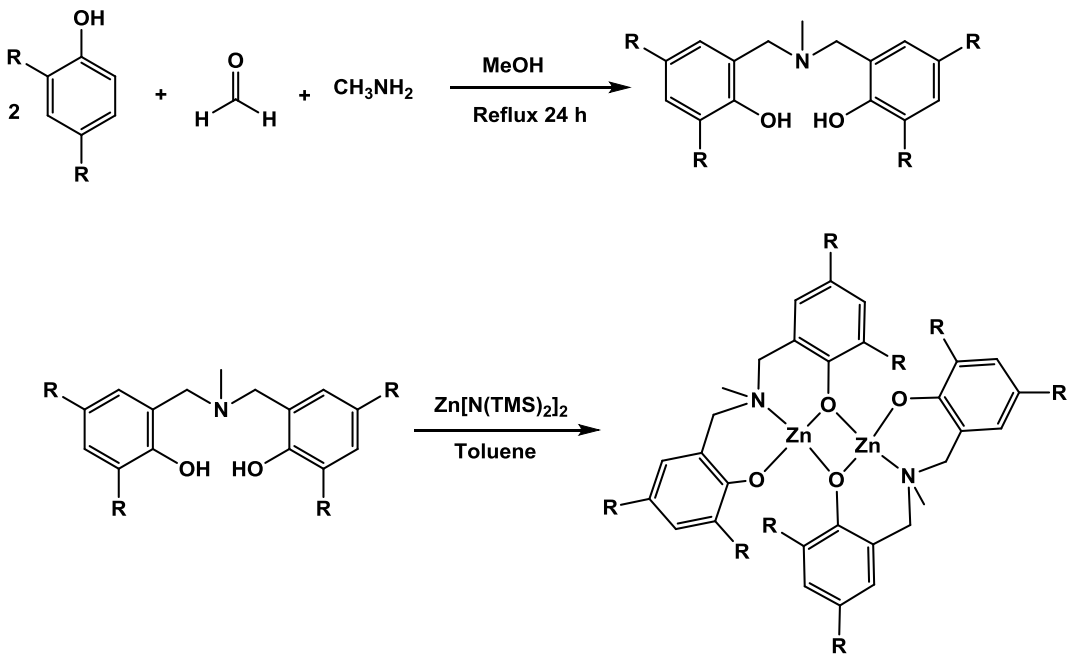


**Scheme 3.1. Synthesis of methylamino-N,N-bis(2-methylene-4,6-di-*tert*-butylphenol ($H_2L1$) and its reaction with a $Zn^{2+}$ source.**

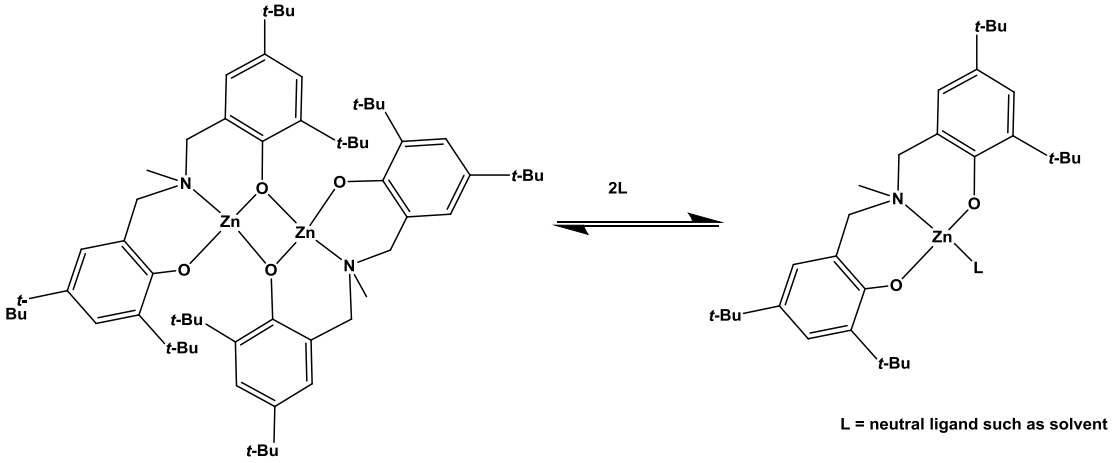


**Scheme 3.2. The equilibrium equation between the dimeric complex $[Zn(L1)]_2$ and the monomeric complex in the presence of a donor ligand.**

3.1.2. Attempted synthesis of a benzylated version of **$H_2$L1**.

We attempted to synthesize a variant of **$H_2$L1** by using benzylamine instead of methylamine. Unfortunately, the desired ligand was not produced. Instead, a cyclic benzoxazine was formed (see section 2.2.1). It was surprising that such a minor modification of the starting material led to such a different product.

3.1.3. Synthesis of a bis(2-picolyl)amine (BPA) complex of $Zn^{2+}$

Commercially available bis(2-picolyl)amine (BPA, **L2**) was also studied as a potential ligand to develop an zinc-enzyme active site structural and functional mimetic. BPA has been identified as a promising ligand in ITC studies. BPA is a tridentate ligand that can potentially bind $Zn^{2+}$ with two pyridine nitrogen atoms and the nitrogen of the secondary amine. The Zn(BPA)$Cl_2$ was synthesized at 60 °C using commercially purchased bis(2-picolyl)amine and zinc dichloride dissolved in methanol. The product was isolated and was confirmed as Zn(BPA)$Cl_2$ by obtaining spectral data that matched literature values.[16] Zn(**L2**)$Cl_2$ is well known and its crystal structure has been reported.[17] No evidence was observed for other binding modes of BPA (such as a 2:1 BPA:Zn ratio) in the sample of Zn(**L2**)$Cl_2$ that was synthesized and used in the studies.

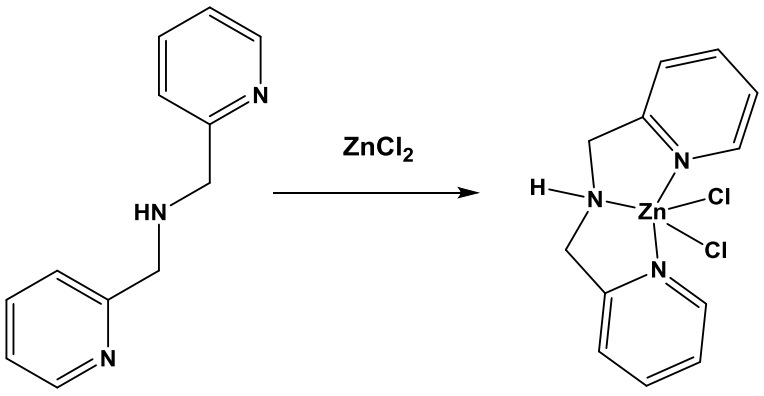


**Scheme 3.3. The reaction of the tridentate bis(2-picolyl)amine (BPA) and $ZnCl_2$.**

3.1.4. Previously synthesized (ZnL) Species

$Zn(Tp^{Ph,Me})OH$ and $Zn(Tp^{Ph,Me})(8HQ)$ have been previously reported in the Dr. Grice group and were used in this study.[13] In addition, a previously unreported ligand (**L4**) and its zinc complex were also examined. **L4** was synthesized by Mark Gudger in the Grice lab according to the following reaction and has been characterized by $^1H$ NMR, elemental analysis and X-ray crystallography (unreported data).

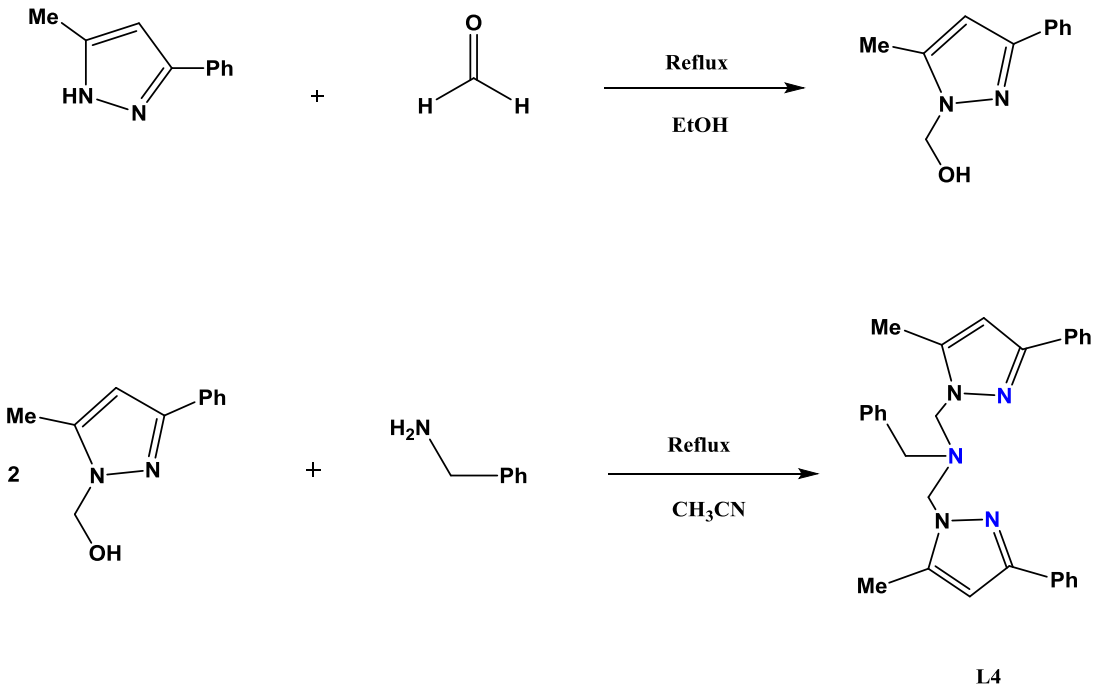


L4

**Scheme 3.4. The synthesis reaction of L4. The nitrogen atoms in blue in L4 are the donors in the ligand that coordinate to $Zn^{2+}$.**

3.2. Examining the hydrolytic activity of Zn-ligand complexes

The amide bond is ubiquitous in nature. They are the key chemical linkages in peptides such as proteins, enzymes, and antibodies. The resonance structures of amides explain many of the properties of this functional group, such as the short (N−C(O)) bond length, barrier to

N−C(O) rotation, planar geometry, IR stretching frequencies, $^{13}C$ NMR chemical shifts, and resistance toward nucleophilic attack.[19] Most biological reactions are catalyzed by enzymes, including hydrolysis of proteins, fats and carbohydrates. Although amides can readily be cleaved by enzymes such as proteases, it is difficult to selectively break the carbon–nitrogen bond of an amide using standard organic chemistry.[20] Transition-metal-catalyzed cleavage of inert chemical bonds such as C−H, C−C, and C−O bonds is an important area of organic chemistry and organometallic chemistry.

The cleavage of amide C−N bonds, especially by transition-metals, was initially reported in 1980, and has become an area of focus since 2010. It provides a mild and convenient approach to obtain nitrogen and/or carbon sources for the synthesis of valuable products.[21] Here we attempted to determine if amide carbon–nitrogen bonds can be activated and cleaved using ligand-$Zn^{2+}$ binary complexes that had been identified as potential HDAC structural mimics. We wished to determine if the Zn-ligand complexes have the ability to function as an enzyme. Transition-metal-catalyzed C−N bond cleavage is classified into five approaches: (1) via oxidative addition of transition-metal catalysts to C−N bond, (2) via imine or iminium species, (3) via ammonium species, (4) via β-amino elimination, and (5) via insertion/deinsertion.[21] Two types of C−N bonds, including the amide C−N bond and the non-carbonyl C−N bond, are involved in an amide molecule. Generally, the amide C−N bond is considered to be more reactive than the non-carbonyl C−N bond. Another factor to consider in this process is sterics. An amide bond that is less sterically hindered by substituents is more likely to be cleaved.[22] In Scheme 3.5 the mechanism of hydrolyzing an amide bond by a Zn-ligand complex with a bound hydroxide is shown.

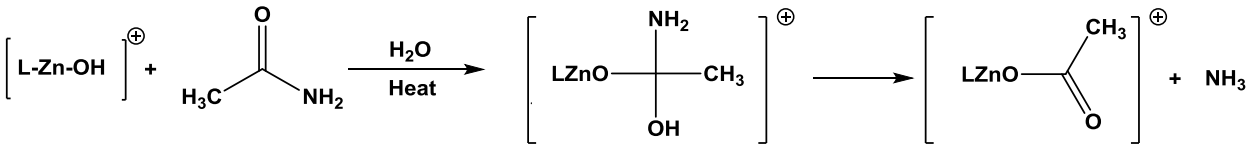


**Scheme 3.5. The mechanism of hydrolyzing an amide bond by a Lewis acidic $Zn^{2+}$.**

We used N-benzylacetamide as a model for the substrate of *Histone Deacetylase*. The hydrolysis of benzylacetamide was not successful at room temperature. Therefore, the reaction was performed in an 100 $^{\circ}$C oil bath with a variety of catalysts. The $^{1}$H NMR spectra of the solutions were collected at different times of the reaction (Scheme 3.6).

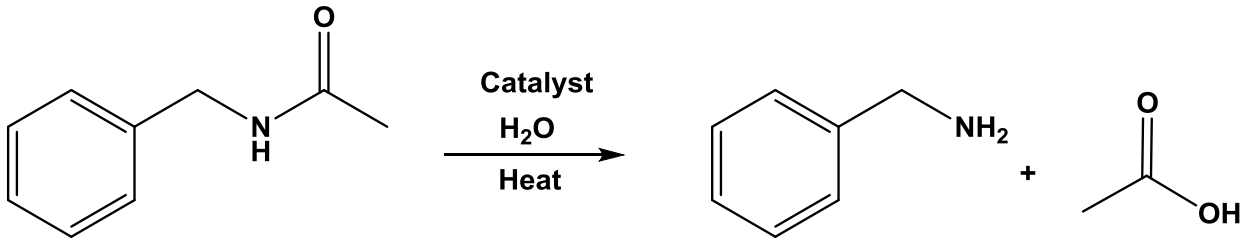


**Scheme 3.6. The hydrolysis reaction of benzylacetamide in the presence of $H_2O$ and catalysts (ZnL) with heat.**

In order to determine whether the reaction between Zn-ligand and amide compound occurred, the $^{1}$H NMR spectra for the amide starting material and benzylamine were taken as reference spectra. We examined the hydrolysis of benzylacetamide using four Zn-ligand complexes, $ZnCl_2$ and an $Al^{3+}$ compounds in a 1:1 mixture of water and DMSO-$d_6$ (for solubility and NMR locking purposes). The data is shown in Table 3.1.

**Table 3.1. Hydrolysis attempts for benzylacetamide in the presence of various catalysts**.

| Complexes | Temperature (°C) | Time | Result |
|---|---|---|---|
| **Zn(L1)** | 60-100 | >2 weeks | No hydrolysis |
| **Zn(L2)** | 100 | > 3 weeks | No hydrolysis |
| **Zn(L3)** | 100 | > 3 weeks | No hydrolysis |
| **$ZnCl_2$** | 100 | > 3 weeks | No hydrolysis |
| **Zn(L4)** | 100 | > 3 weeks | No hydrolysis |
| **$Al(NO_3)_3 \cdot 9H_2O$** | 100 | > 3 weeks | Some hydrolysis |

Unfortunately, none of the zinc complexes tested showed clear evidence for C−N bond cleavage under the reaction conditions studied. Using $Al^{3+}$ in the form of aluminum nitrate nonahydrate, $Al(NO_3)_3 \cdot 9H_2O$, some hydrolysis was observed after extended heating in pure $D_2O$, rather than a mixture of DMSO and water. These results highlight the stability of amide bonds and show that while the zinc complexes studied in this work may be *structural* models for the enzymes of interest, they are not *functional* mimics of hydrolase enzymes. Although the identity of the atoms in the 1$^{st}$ coordination sphere are the same or similar as in HDAC and other hydrolyase enzymes, the exact positioning of these atoms are most likely not the same. In addition, though $Zn^{2+}$ is important to catalysis, the enzyme catalytic active site provides catalytic amino acid residues positioned in ideal locations to interact with the substrate and lower transition states through acid-base interactions. In our complexes, these additional residues are not present, so the substrate has to compete with other ligands to bind to the metal and likely has much higher reaction barriers to overcome. These are major reasons why trying to mimic

enzyme active sites with small molecules is so challenging

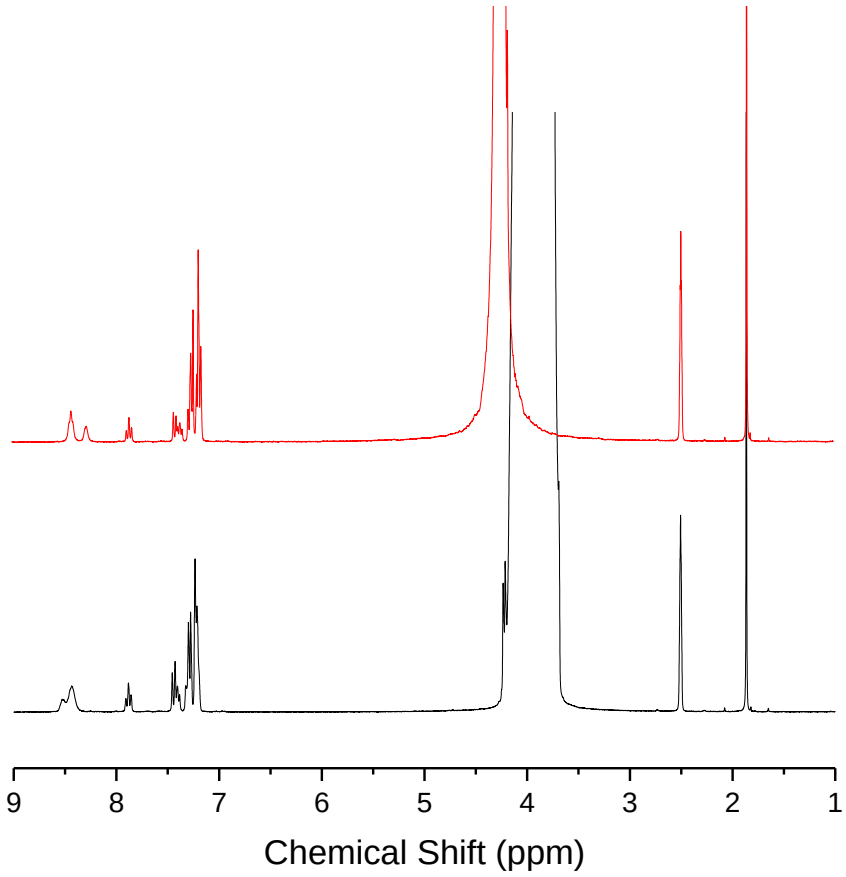


**Figure 3.1. $^{1}$H NMR spectra of the hydrolysis reaction mixture of amide substrate and Zn(L2) in DMSO, in the presence of water and heat.** Spectrum in black was collected after 24 h and the spectrum in red was collected after 3 days in an oil bath (100 ºC). Comparing these spectra with the spectrum of benzylamine, it appeared that there was no sign of amine formation.

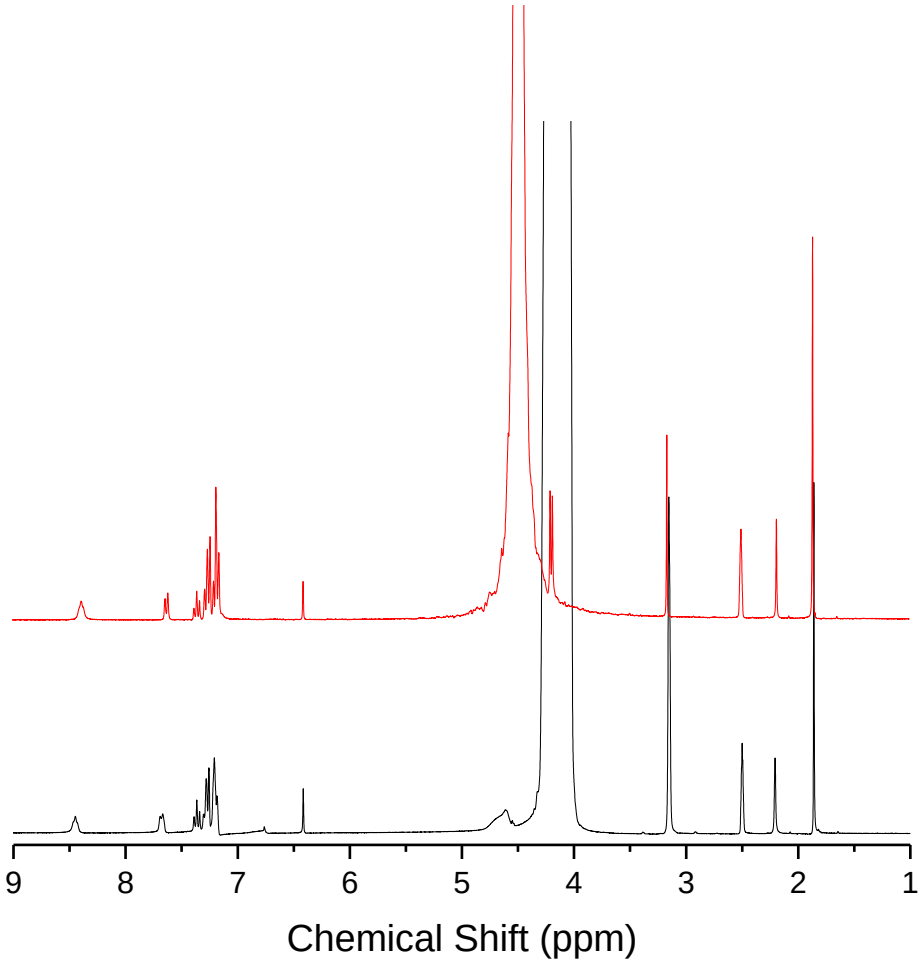


**Figure 3.2. The $^{1}$H NMR spectra monitoring the hydrolysis of amide substrate with Zn(L3)OH in DMSO, in the presence of water and heat**. The spectrum in black was collected after 24 h and the spectrum in red was collected after 3 days in an oil bath (100 ºC). Comparing these spectra with the spectrum of benzylamine, it appeared that there is no sign of amine formation.

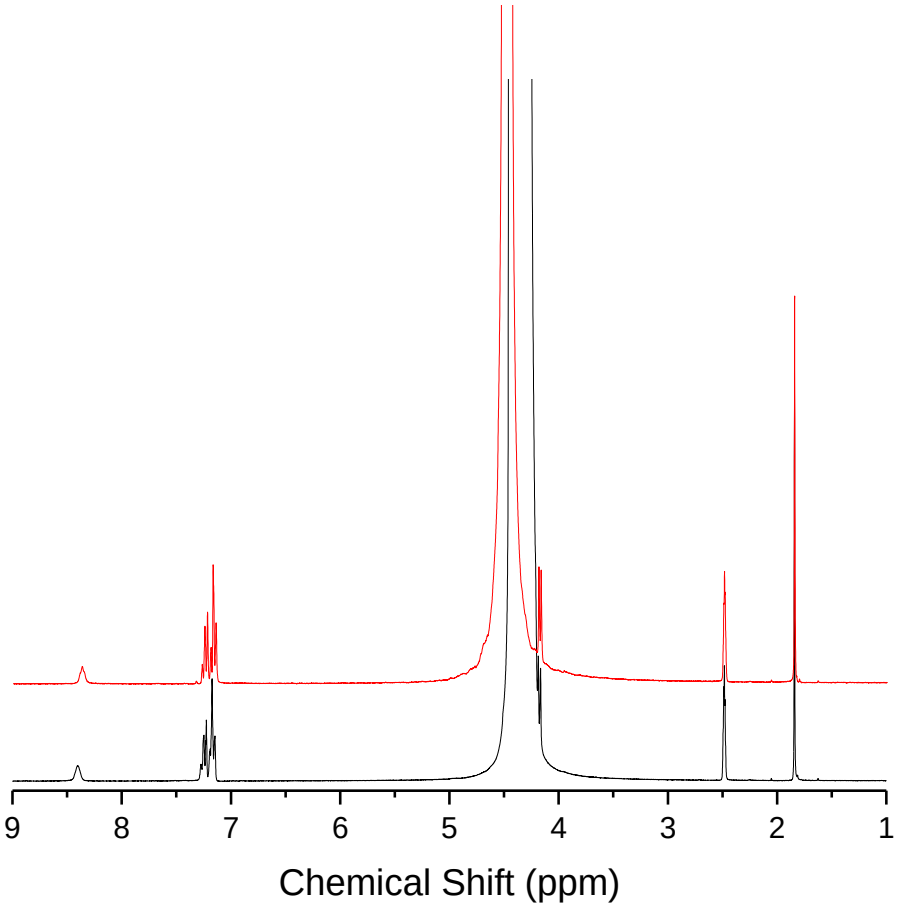


**Figure 3.3. The $^{1}$H NMR spectra for the reaction of $ZnCl_2$ and amide complex in the presence of water and heat.** The lower spectrum in black was taken at 24 h, and the above spectrum in red was taken after 3 days in the oil bath. As shown, no evidence of amine product is present.

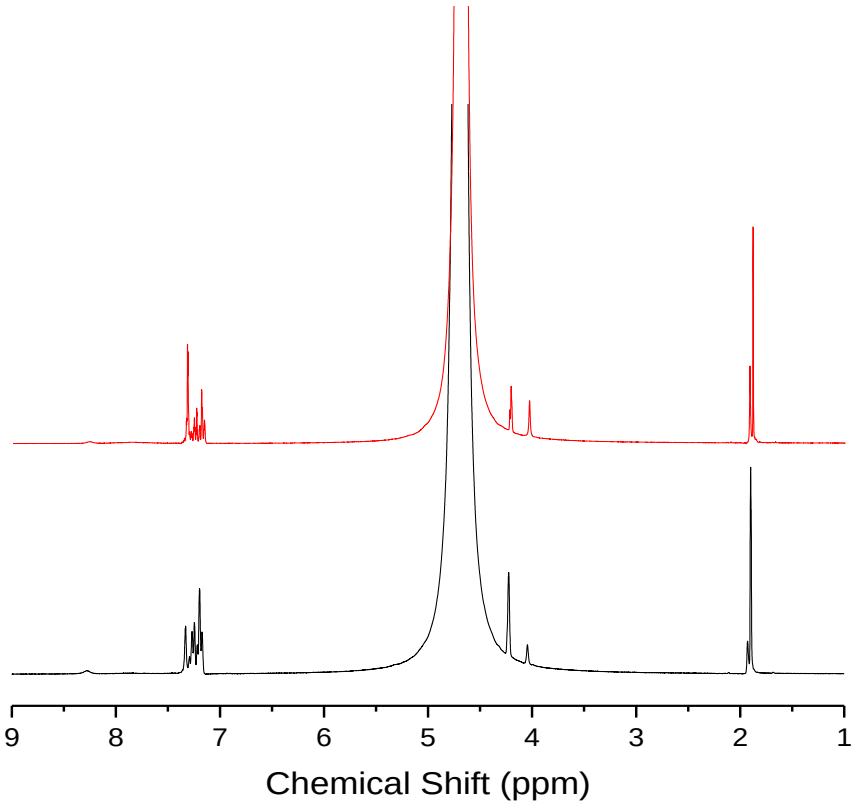


**Figure 3.4. $^{1}$H NMR spectra monitoring the reaction of $Al(NO_3)_3 \cdot 9H_2O$ with amide in presence of water and heat**. The mixture was dissolved in $D_2O$ (deuterium oxide). Heat was applied to the reaction with an oil bath (100 ºC) and the spectrum in black was taken of the reaction after 22 h. The spectrum in red was taken of the reaction after approximately one month. The appearance of benyzlamine was observed, but complete hydrolysis did not occur even after a month of heating.

3.3. Studies of interaction of $Zn^{2+}$-ligand complexes with inhibitors

3.3.1. Zn(**L1**) with Vorinostat (SAHA)

Many HDACIs share the same pharmacophore structure shown in Figure 1.4, which consists of a zinc binding group (ZBG) that chelates the zinc ion, a capping group that caps the active site binding pocket, and a linker between the ZBG and the cap. One ZBG of interest is the hydroxamic acid functional group present in SAHA, because of its significant binding ability to zinc ions. However, inhibitors with these coordinating groups can cause severe toxicity due to their nonspecific chelation to metals.[23,24] Other HDACIs have been discovered that are far more potent than SAHA, but are also typically more toxic as revealed in *in vivo* studies.[25] SAHA is one of the most commonly used HDACIs, targeting multiple HDAC enzymes, which makes it difficult to determine if the therapeutic function and the toxicity of SAHA is a result of non-specific binding to biological metals or to inhibiting a specific HDAC or a multiple HDACs.[26]

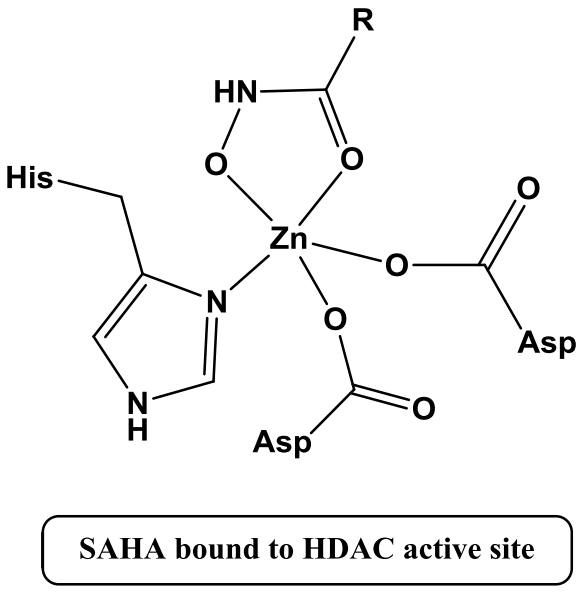


**Figure 3.5. The interaction between $Zn^{2+}$ in HDAC and the hydroxamic acid group in SAHA**. The ligand with the R group is SAHA, and the two histidine and asparagine groups are residues in the HDAC active site coordinating to the hydrolytically active $Zn^{2+}$ ion.

By using computational chemistry (DFT and QM\MM calculations), Chen and co-workers studied the binding of various HDAC inhibitors and $Zn^{2+}$.[27] The results showed that the hydroxamate group has a pKa of 9.4 in solution, and that the aliphatic linker has the ability to form van der Waals interactions with the pocket.[14] When performing experiments with the goal of forming Zn(**L1**)(SAHA), we considered several approaches and analyzed the products via $^1$H NMR, UV-Vis, IR and fluorescence spectroscopies. The first approach was to deprotonate SAHA by adding 1 equivalent of base (KOH and 18-crown-6), and then add 1 equivalent of $[Zn(\mathbf{L1})]_2$ in methanol. The reaction was stirred for 24 hours, but no Zn−SAHA product was formed, as determined by IR and $^1$H NMR spectra. The second approach was to dissolve 1 equivalent of $[Zn(\mathbf{L1})]_2$ and 1 equivalent of SAHA in acetonitrile and heat the reaction at 60 ˚C for 24 h. There was some shifting in the $^1$H NMR spectra, but no clear evidence of product formation. Therefore, the final approach was to elevate the temperature of the oil bath to 100 ˚C for the same reaction. A white solid was formed, and a $^1$H NMR spectrum was taken. Although there was change in $^1$H NMR spectra, the overlapping between the signals of the ligand and the inhibitor made it hard to determine if Zn binding with SAHA has occurred.

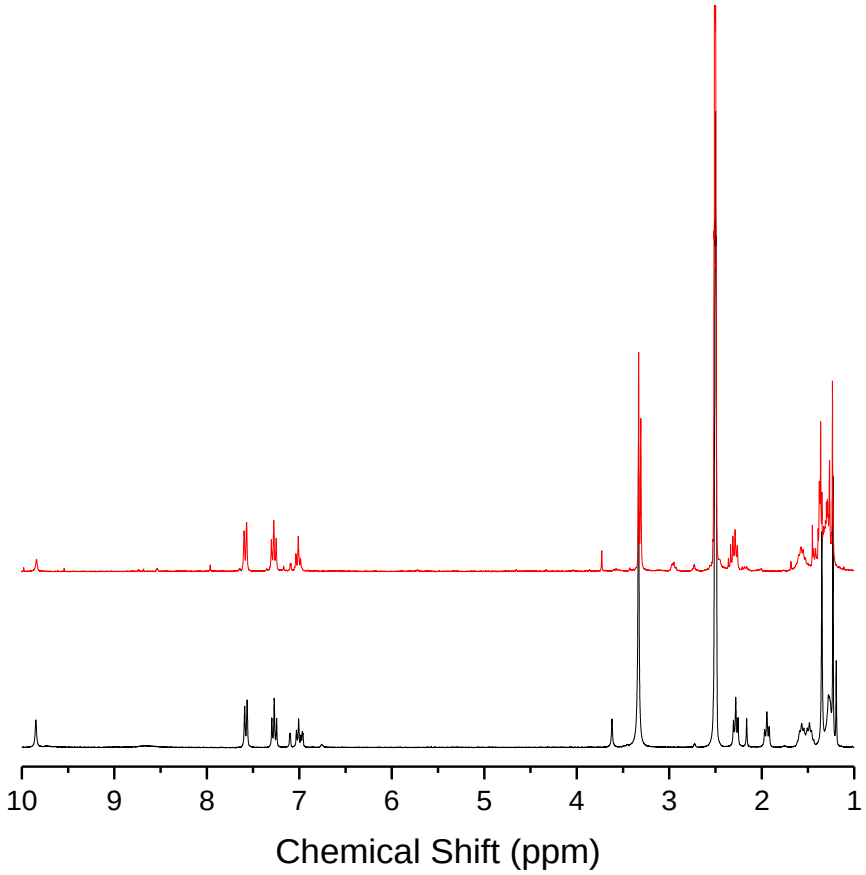


**Figure 3.6. $^{1}$H NMR spectra of Zn(L1) and SAHA at 60 ˚C for 24 h**. The spectrum in black is for the Zn(**L1)** with SAHA before heating. The spectrum in red is for the Zn(**L1**) with SAHA after 40 h under 60 ºC. As indicated before, spectral changes occurred, but the overlapping between signals in the spectra makes it hard to identify the binding between the $Zn^{2+}$ and SAHA.

3.3.2. Zn-Ligand interaction with 8-hydroxyquinoline (8HQ*)*

8-hydroxyquinoline is a well-known strong metal ion chelator with a rich diversity of biological properties that has been shown to be an inhibitor of HDAC2. 8-Hydroxyquinoline binds $Zn^{2+}$ through the phenolic oxygen anion and the pyridinic nitrogen (Figure 3.7).

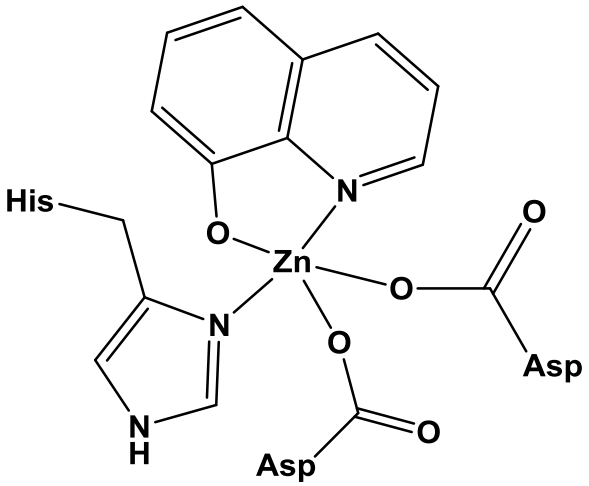


**Figure 3.7. 8-HQ interaction with $Zn^{2+}$ in an HDAC Active Site.**

Reaction between Zn(**L1**) and 8HQ was studied by combining them at 60 ˚C. $^{1}$H NMR spectra were collected (Figure 3.8), and as shown in the spectra, a broad signal appeared at 2.23 ppm, corresponding to water formation with no other major changes observed. The color of the solution changed to yellow, indicating that 8HQ was reacting. However, $^{1}$H NMR spectroscopy did not reveal clear evidence of 8HQ coordinating to the zinc complex. The signals for the 8HQ and the Zn(**L1**) did not shift appreciably enough to make a clear conclusion.

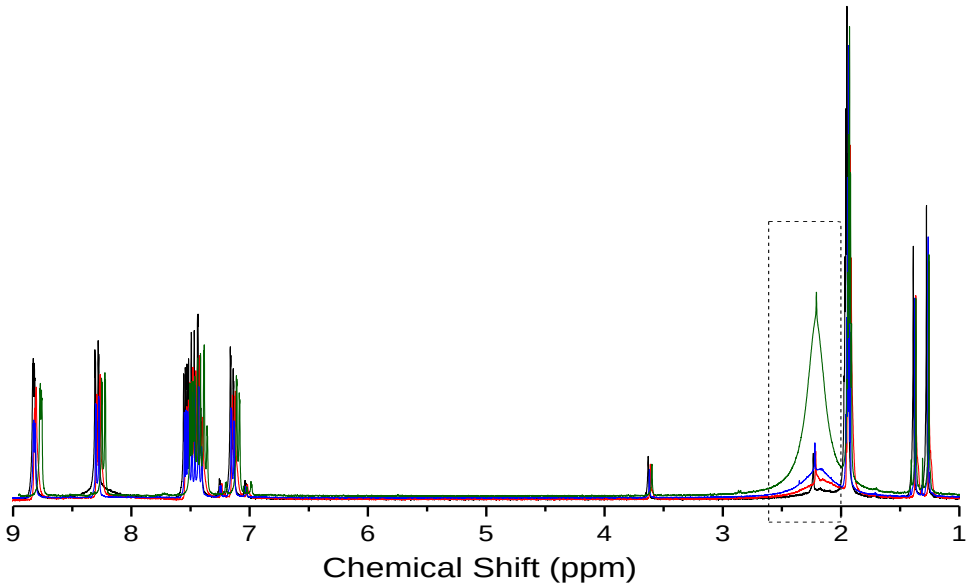


**Figure 3.8. $^{1}$H NMR spectra for Zn-L1 interaction with 8HQ in ACN.** The black spectra were taken before heat was applied to the reaction, the red spectra for the reaction after 21 h in oil bath 60 ˚C, the blue spectra for the reaction after 3 days in oil bath and the green spectra was for the reaction after one week in oil bath. The mixture was yellow before heat applied and the color started to change gradually until it turned to orange.

3.4. Computational studies of the interaction of AHA and Zn(**L1**)

*Ab initio* calculations were performed with the Gaussian 2009 program package.[27] Two zinc complexes were optimized using HF (Hartree-Fock) as well as DFT (Density Functional Theory) levels of theory with a B3LYP functional. Both approaches used a 3-21G basis set.[28] The zinc ion was first bound to the bis(phenolato)amine and methylamino-*N,N*-bis(2-methylene) as shown in Figure 3.9. These ligands are models for **L1**, but without the tert-butyl substituents in order to reduce computational time. Both complexes were successfully optimized in reasonable conformations. Moreover, the optimized Zn-ligand complexes have at least one or

two open sites that could bind with the inhibitor, to form complexes with a tetrahedral or higher geometry.

Bonding of the zinc complexes to an inhibitor was examined with deprotonated acetohydroxamic acid (AHA) as the inhibitor, a small molecule analog of SAHA. As with SAHA, AHA is a bidentate inhibitor that complexes the $Zn^{2+}$ in the HDAC active site through both hydroxamate oxygen atoms. The binding modes that were optimized are shown in Fig 3.10, and the binding energy of each mode was found. The binding mode of the AHA anion in models A and D is mono-dentate, whereas in models B and C, the binding is bidentate. In Table 3.2, the basis set superposition error (BSSE) and the binding energies of $Zn^{2+}$ and the ligand are reported. BSSE-corrected energies of all models differ in terms of the binding structures. In addition, Hartree–Fock calculations are known to underestimate the electron correlation in the molecule; thus, this method may provide incorrect numbers, but is useful to examine in terms of general trends between different complexes. Using HF, models A and D share the same bonding energy of 45.35 kcal/mol. The highest binding energy that was calculated in the HF method is of model C. On the other hand, in the DFT/B3LYP method, model A has the highest energy 73.92 kcal/mol and the lowest number is model D with 45.85 kcal/mol. The DFT/B3LYP approach would be expected to be more accurate than HF, so these numbers are likely closer to the real values. The distances between Zn and O's in models A, B and C are between 2 to 3 Å. It should be noted that models A and D have different distance between the metal and the O in the amide group. In most hydroxamate complexes characterized by X-ray crystallography, the metal-OC bond is longer than metal-ON bond. However, the magnitude of the difference is different among different metal complexes.[29]

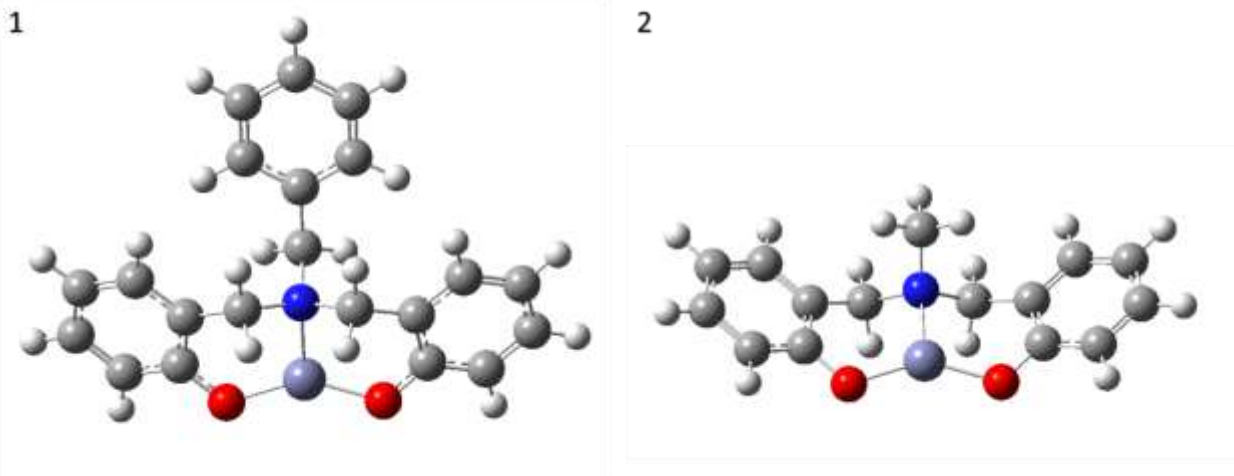


**Figure 3.9. Two different models of the Zn(L) species: Zn(2,2'[[(phenylmethyl)imino] bis(methylphenol)]) (Zn-L(Me) (1) and Zn (2,2'[[(methyl)imino]bis(methylphenol)] Zn-L(Ph) (2)**. Both complexes shown were calculated in gas phase via HF level of theory with a 3-21G basis set. Atoms are labeled by color, where red atoms are O, blue atoms are N, purple is the $Zn^{2+}$, gray are C atoms, and white are H atoms.

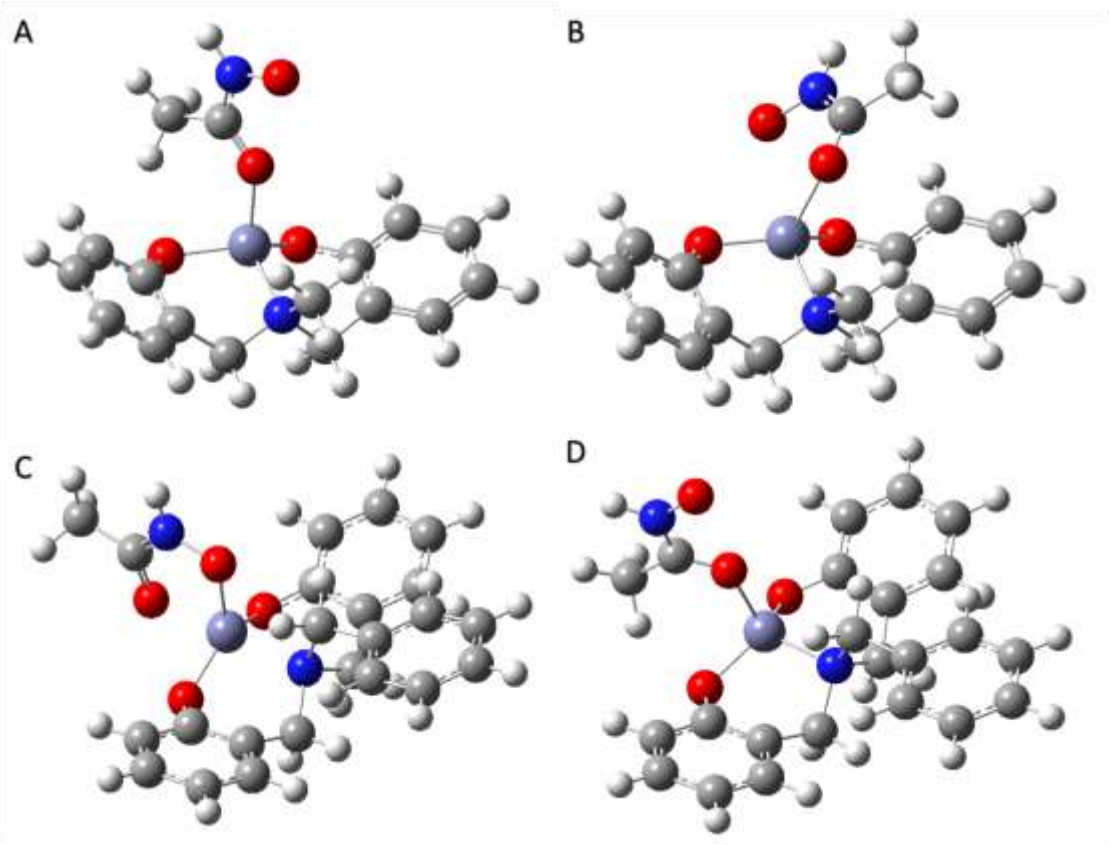


**Figure 3.10. Four different models of the Zn-Ligand-AHA species**. A) HF optimized structure, AHA C-O site bonding with Zn-L complex (1), B) HF optimized structure, AHA C-O site bonding with (ZnL) complex (2), c) HF optimized structure, AHA N-O site bonding with (ZnL) complex (1) and D) HF optimized structure, AHA C-O site bonding with (ZnL) complex (2). The DFT/B3LYP structures were similar, but with slightly different distances.

**Table 3.2. BSSE-corrected Binding Energies of $Zn^{2+}$ and the ligand**

| | **Zn-L(Me) (1) kcal/mol** | **Zn-L(Ph) (2) kcal/mol** |
|---|---|---|
| **HF/3-21G** | 213.49 | 213.47 |
| **B3LYP/3-21G** | 126.07 | 131.75 |

**Table 3.3. BSSE-corrected Binding Energies of Zn-Ligand complexes with**

| | **Model A kcal/mol** | **Model B kcal/mol** | **Model C kcal/mol** | **Model D kcal/mol** |
|---|---|---|---|---|
| **Chelating** | Monodentate | Bidentate | Bidentate | Monodentate |
| **HF/3-21G** | 45.35 | 44.42 | 49.21 | 45.35 |
| **B3LYP/3-21G** | 73.92 | 68.63 | 73.50 | 45.85 |

**Table 3.4. The distances between Zinc and the AHA oxygens.**

| | **HF/3-21G (Å)** | | **B3LYP/3-21G** (Å) | |
|---|---|---|---|---|
| **Zn-L AHA** | Zn-ON | Zn-OC | Zn-ON | Zn-OC |
| **Model A** | 4.59 | 2.69 | 1.91 | 2.56 |
| **Model B** | 2.82 | 1.99 | 2.11 | 1.99 |
| **Model C** | 2.02 | 3.42 | 1.92 | 2.05 |
| **Model D** | 4.59 | 1.97 | 4.662 | 1.95 |

In conclusion, several structural mimetic complexes of HDAC were synthesized and characterized. These complexes were found not to be functional mimetics of HDAC because they show no activity towards hydrolyzing amide bonds. However, $Al(NO_3)_3 \cdot 9H_2O$ was used as an alternative metal to hydrolyze amide bonds without the presence of a supporting multidentate ligand. The interaction of zinc complexes and inhibitors were examined by $^1H$ NMR, but the spectra were hard to analyze due to the overlapping signals. This indicates that the $^1H$ NMR is not an ideal choice of spectroscopy to study the interactions. As shown in the following chapter, UV-Vis and fluorescence spectrometry were found to be more promising. Finally, a computational study of Zn(**L1**) was performed by using two different approaches HF and

DFT/B3LYP, both using the 3-21G basis set. Calculations were performed on the interaction between Zn-Ligand compounds and AHA. Four different models were optimized and their binding energies were determined. The computational data reveal that the inhibitor (AHA) binds the metal most favorably in a bidentate fashion. However, given the low basis set and the use a gas phase conditions, the numbers in this study cannot be directly compared to experimental information. The binding affinities of the ligands and inhibitor to $Zn^{2+}$ need to be calculated by using more advanced methods (functional benchmarked for zinc complexes, larger basis sets, solvation models, etc.) to obtain values that can be directly comparable to experimental data.

## Chapter 4. Examining the binding between $Zn^{+2}$ and ligands and inhibitors using UV-Vis and fluorescence spectroscopies

### 4.1. Determining the binding affinities between the $Zn^{2+}$ and ligands and Zn-ligand complexes with inhibitors using UV-Vis spectroscopy

#### 4.1.1. Introduction

UV-Vis spectroscopy is a common technique to monitor molecular interactions or chemical reactions. In spectroscopically monitored titration experiments, the association constant ($K_a$) between a ligand and a metal ion can be determined from changes in the parameters of the spectra, such as wavelength of maximum absorbance ($\lambda_{max}$) and molar absorptivity ($\varepsilon$). [30] Typically, a titration is performed by holding the concentration of one species constant (in our case the Zn-ligand complex), while increasing the concentration of the other species ($Zn^{2+}$), keeping overall volume nearly the same. In our studies, we applied this concept to determine the association constant between $Zn^{2+}$ and a ligand from the spectra after adding one aliquot of a $Zn^{2+}$ source to a Zn-ligand complex in solution.

The basis for this type of analysis is Beer's Law, applied at the $\lambda_{max}$ of the absorption of the Zn-ligand complexes.

Beer's Law is defined as:

$$A = \varepsilon bc \qquad (1)$$

In which A is the absorbance (unitless, sometimes called "arbitrary units"), ε is the molar absorptivity with units of L $mol^{-1}$ $cm^{-1}$, b is the path length of the sample (which is 1 cm for all samples), and c is the concentration of the compound in solution in mol $L^{-1}$. Note that $\varepsilon$ is dependent on the wavelength selected for a measurement, and will be different for a different

wavelength even if all else is constant. Given a constant cell path length and the same wavelength of absorption, the absorbance will be linearly related to the concentration of the species under study *if Beer's Law is valid*. Beer's Law is only valid in the so-called "linear regime", where absorbance varies linearly with concentration. This relationship breaks down as absorbance increases above ~1.0. In general, this is because so little light is transmitted that changes in the amount transmitted are difficult to determine. Further discussion of the details of Beer's law and the non-linearity issues will not be covered in this thesis.

The binding or association constant ($K_a$) corresponds to the reaction $Zn^{2+} + L \rightleftharpoons ZnL$ and can be easily determined if the concentrations of all components are known at equilibrium. Given that all of the individual concentrations of the species are difficult to determine in a complex solution mixture, we can consider the opposite reaction, which occurs when Zn(L) is dissolved in solution (see table 4.1), to obtain the $K_a$ value. The process is explained in the following text. If the formal concentration of the zinc-ligand complex in solution is $[ZnL] = C_0$, and the concentration change upon dissociation is $[\mathrm{ZnL}] = -\mathrm{x}$, then the final concentration when dissolved in solution will be $[\mathrm{ZnL}] = \mathrm{C_0} - \mathrm{x}$.

$$ZnL \rightleftharpoons Zn^{2+} + L$$

**Table 4.1. The concentration of each product and reactant in the equilibrium reaction.**

| | **(ZnL)** | **$Zn^{2+}$** | **L** |
|---|---|---|---|
| **Expected concentration ($C_\circ$)** | $C_\circ$ (known) | 0 | 0 |
| **After equilibrium shift upon dissolving in solution** | -x | +x | +x |
| **The equilibrium concentration** | $C_\circ$ -x | x | x |

In this study, the change in initial concentration the Zn(L) complex is reflected in the absorbance according to Beer's Law:

$$A_1 = \varepsilon b(C_0 - x) \qquad (2)$$

Where the value $A_1$ is the absorbance observed after Zn(L) was dissolved in solution. This absorbance is a result of the *actual* concentration of Zn(L) and x is the concentration of the dissociated amount of Zn(L) in solution. We are assuming that when a Zn(L) species is added to solution, some of the ligand dissociates according to $Zn(L) \rightleftharpoons Zn^{2+} + L$. When adding an excess of an additional $Zn^{2+}$source such as $ZnCl_2$, Le Chatlier's principle should result in re-forming all of the Zn(L) species. The Beer's Law equation will then become:

$$A_2 = \varepsilon b(C_\circ) \quad (3)$$

Where $A_2$ is the absorbance after sufficient amount of $Zn^{2+}$ is added to drive all free ligand to completely form (ZnL). Therefore, the change in absorbance (ΔA) between the absorbance of just Zn(L) ($A_1$) and the absorbance after adding $Zn^{2+}$ to Zn(L) ($A_2$) will be:

$$\Delta A = A_2 - A_2 = \varepsilon b(x) \qquad (4)$$

The molar absorptivity (ε) of the starting Zn(L) complex at the wavelength used is necessary for concentration calculations and be determined as follows:

$$\varepsilon = \frac{A_2}{bC_0} \qquad (5)$$

Once the molar absorptivity for a complex is obtained at the specific wavelength of study, the change in absorbance can been used to find the chance in concentration (x), using equation (6):

$$x = \frac{\Delta A}{\varepsilon b} \qquad (6)$$

In order to calculate the binding constant $K_a$, the increase of absorbance after adding $Zn^{2+}$ was obtained by subtracting the absorbance of the (ZnL) from the absorbance after additional $Zn^{2+}$. The $K_a$ was estimated by using the equations above and Table 4.1 combined in the equilibrium expression:

$$K_a = \frac{(Zn(L))}{(Zn^{2+})(L)} = \frac{\left(\frac{A_\circ}{\varepsilon b}\right)}{\left(\frac{\Delta A}{\varepsilon b}\right)\left(\frac{\Delta A}{\varepsilon b}\right)} \qquad (7)$$

$$K_a = \frac{A_\circ . \varepsilon}{(\Delta A)^2} \qquad (8)$$

Acetonitrile (ACN) was used as a solvent in some of the reactions due to the favorable short wavelength cutoff of 190 nm.[30] All of the components in this study are soluble in ACN. In some cases, it was possible to use the same buffer solutions used in previous ITC experiments.[16] Analysis of the data was performed using Origin Lab software.

In addition to examining the (ZnL) interaction, we also examined the Zn-ligand interaction with inhibitors using UV-Vis spectroscopy and fluorescence spectroscopy. The chapter is divided in two sections based on the two approaches (UV-Vis and fluorescence spectroscopies) through which the interaction between $Zn^{2+}$ and the ligands and between the Zn-ligand complexes and the inhibitors were analyzed.

4.1.2. UV-Vis spectra for the interaction between $Zn^{2+}$ and ligands

UV-Vis spectroscopy was used to examine zinc with several ligands. As shown in table 4.2, the binding constant $K_a$ values were generally in the range of $10^5$–$10^7$ $M^{-1}$ with a few

outliers. The binding constant for BPA (**L2**) in buffer was close to the values from ITC, which validates our results from this absorbance study.[16] This also confirms that the affinity of the ligand to bind with $Zn^{2+}$ is strong enough to be stable in further reactions with inhibitors.

**Table 4.2. Binding values between zinc and ligands studied using UV-Vis spectroscopy.**

| | Solvent | $C_o$(M) | ΔA | $A_2$ | ε | x (M) | $ZnCl_2$ (mg) | $K_a$ ($M^{-1}$) | $\lambda_{max}$ (nm) |
|---|---|---|---|---|---|---|---|---|---|
| **Zn(L1)** | ACN | 0.0010 | 0.011 | 1.26 | 1300 | $9.4\times10^{-6}$ | 7.0 | $1.2\times10^{7}$ | 280 |
| **Zn(L2)** | Buffer | 0.0010 | 0.029 | 1.48 | 1700 | $2.0\times10^{-5}$ | 7.0 | $3.3\times10^{6}$ | 260 |
| | Buffer | 0.0020 | 0.0093 | 2.57 | 1300 | $7.3\times10^{-6}$ | 7.0 | $3.7\times10^{7}$ | 260 |
| | Buffer | 0.0050 | 0.061 | 2.95 | 5700 | $1.0\times10^{-4}$ | 7.0 | $4.2\times10^{5}$ | 260 |
| | Buffer | 0.50 | 0.14 | 2.95 | 5.5 | $2.5\times10^{-2}$ | 7.0 | $6.9\times10^{2}$ | 260 |
| **Zn(L4) +($ZnCl_2$)** | ACN | 0.0020 | 0.068 | 1.69 | 810 | $8.0\times10^{-5}$ | 7.0 | $2.9\times10^{5}$ | 250 |
| **Zn(L4) +$Zn(OAc)_2$** | ACN | 0.0020 | 0.0015 | 1.31 | 660 | $2.3\times10^{-6}$ | 7.0 | $3.8\times10^{8}$ | 250 |

In general, each spectra of each Zn component increases after adding an excess amount of $Zn^{2+}$ and the maximum absorbance increases, corresponding with an increase in the concentration of the species. Notably, the absorbances of these compounds showed some differences. In Figure 4.1, the UV-Vis spectra of Zn(**L1**) showed one major absorbance. However, in Figure 4.2 there are multiple different peaks for Zn(**L2**)$Cl_2$ in the absorbance. This is because of the overlapping in absorptions that happen at different electronic states. As shown in Figure 4.1 the $\lambda_{max}$ absorbance for Zn(**L1**) is at 280 nm. After adjusting the baseline, the absorbance spectrum was increased by 0.011 after the addition of $ZnCl_2$. Therefore, using equation (7), the association constant $K_a$ is $1.2\times10^{7}$ $M^{-1}$, if we take into account the 1:1 binding.

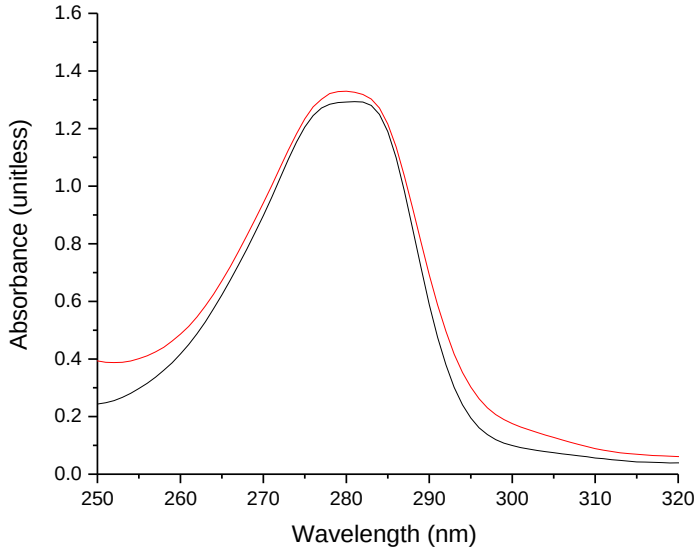


**Figure 4.1. The UV-Vis spectra of Zn(L1)**. The $\lambda_{max}$ = 280 nm and the absorbance spectra of the Zn(**L1**) dissolved in 5 ml acetonitrile has an absorbance of 1.29 (black). The red spectra show absorbance (with a value of 1.32) after adding $ZnCl_2$ (7.0 mg) at the same $\lambda_{max}$.

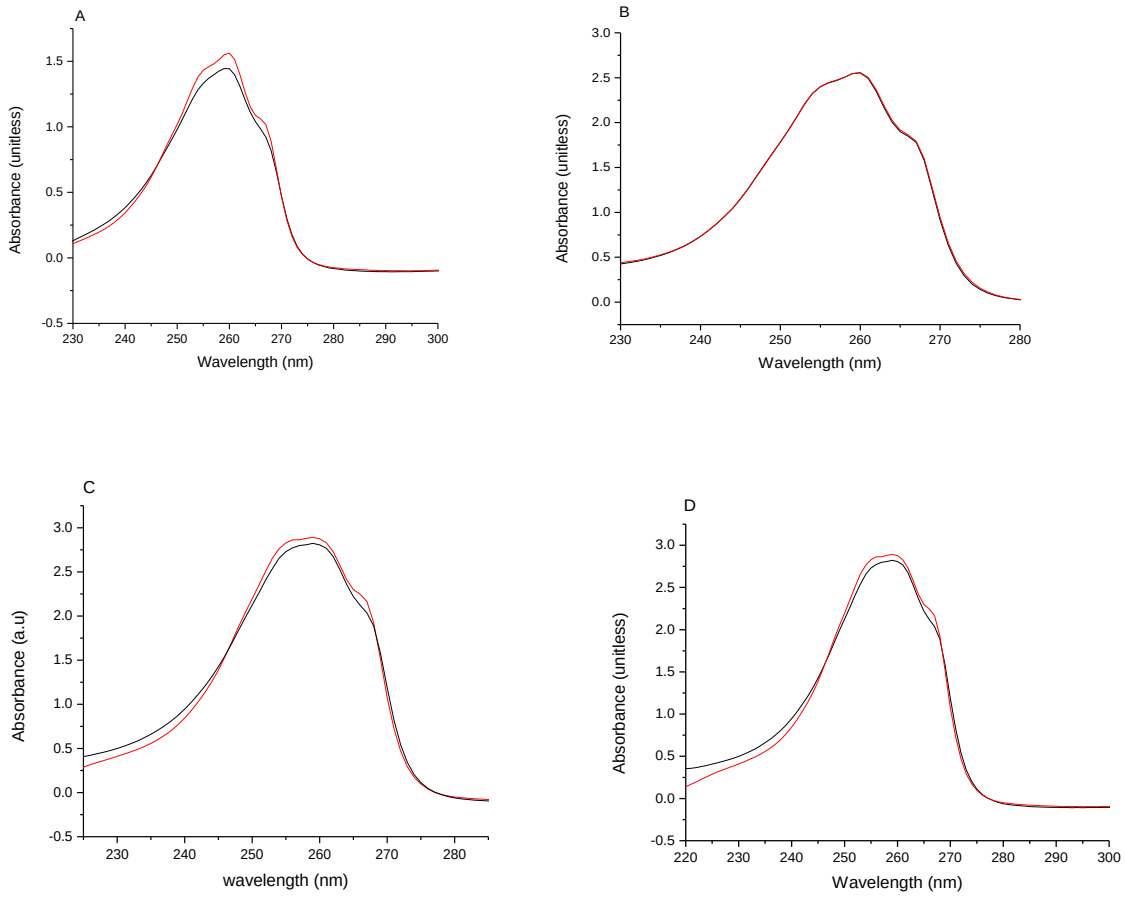


**Figure 4.2. UV-Vis spectra of Zn(L2) with concentrations of 1 mM, 2 mM, 5 mM and 500 mM (A, B, C, and D, respectively).** Spectra in black show the asborbance of Zn(**L2**), with absorbances are at 1.69, 2.55, 2.89 and 2.89 respectively. The red spectra show the absorbance of Zn(**L2**) with the additional of $ZnCl_2$, with absorbances at $\lambda_{max}$ increasing by 0.05, 0.004, 0.07 and 0.16 respectively. All products were disoloved in 5 ml buffer.

The equilibrium association constant obtained from ITC experiments for Zn(**L2**) ($2.4\times10^7\ M^{-1}$) was close to those obtained by UV-Vis experiments.[16] With increasing the concentration of Zn(**L2**), the absorbance increases, because of Beer's Law. However, at higher concentrations Beer's law may not be valid.[30] Four concentrations of Zn(**L2**) were examined in buffer:1 mM, 2 mM, 5 mM and 500 mM. All spectra showed $\lambda_{max}$ of 260 nm with increasing values of absorbance. The Zn(**L2**) shows a $K_a$ of $3.3\times10^6\ M^{-1}$, $3.7\times10^7\ M^{-1}$, $4.2\times10^5\ M^{-1}$ and $6.9\times10^2\ M^{-1}$,

respectively from these four concentrations. The $K_a$ values derived from runs with absorbances > 2 are probably incorrect due to deviations from Beer's Law. At these high absorbances, the percent of total transmitted light becomes very low, so attempting to observe accurate changes in the amount of that light is not possible.

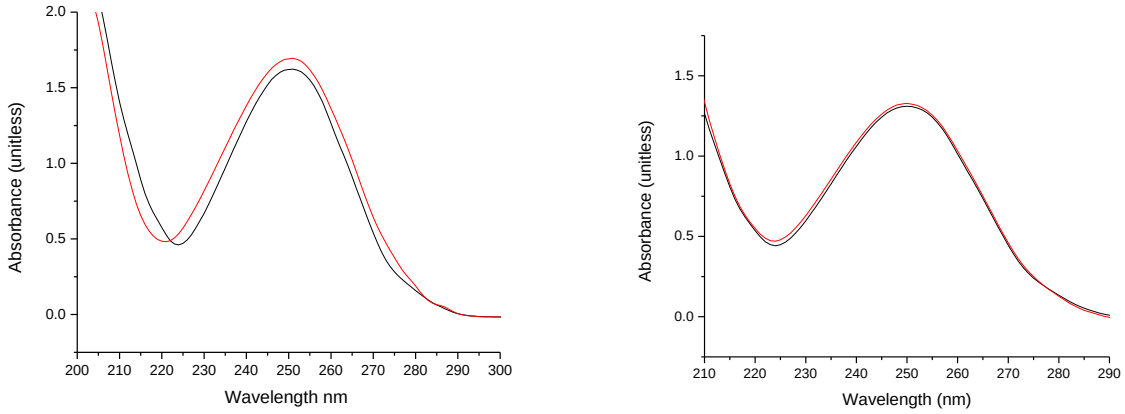


**Figure 4.3. The UV-Vis spectra of Zn(L4) .** The $\lambda_{max}$ is 250 nm and the absorbance at $\lambda_{max}$ is 1.62 (black). The addition of $Zn^{2+}$(red) as $ZnCl_2$ increases the spectra by 0.070 at the same wavelength (plot on the left). The spectra on the right, show the spectra of Zn(L4) at the same concentration, but with added $Zn(OAc)_2$. The $\lambda_{max}$ is 250 nm and the absorbance increases by 0.01.

We were curious to see how different zinc salts might affect the UV-Vis measurements. When $ZnCl_2$ was used with Zn(**L4**), the $K_a$ was ca. $2.9\times10^5$ $M^{-1}$. However, with the addition of $Zn(OAc)_2$, the absorbance increases by 0.018 and the association constant was $3.8\times10^8$ $M^{-1}$, higher in value than using $ZnCl_2$. These numbers are estimates, and show that care must be taken when making comparisons between systems to use the same zinc source. In addition, large

absorbance values (> 1) have so little transmittance that the numbers become less accurate and Beer's law may not be valid. Therefore, these numbers should be calculated again with more dilute solutions in future studies. The rows in Table 4.2 with final absorbance values above 2 are likely not useful runs.

In order to check our assumption that adding $Zn^{2+}$ resulted in complete reformation of Zn(L), we calculated the amount of dissociation of Zn(L) in the presence of $ZnCl_2$ using the $K_a$ values we obtained (see Table 4.2). The equilibrium reaction is shown below, along with table 4.3, which includes a term for the concentration of added $Zn^{2+}$ (z).

$$Zn^{2+} + L \rightleftharpoons ZnL$$

Table 4.3. **The concentration of each product and the reactant in the equilibrium reaction after adding $ZnCl_2$.**

| | **$Zn^{2+}$** | **Ligand** | **(ZnL)** |
|---|---|---|---|
| **The concentrations after adding $ZnCl_2$** | z | 0 | $C_o$ |
| **After equilibrium shift upon dissolving in solution** | +y | +y | -y |
| **The equilibrium concentration** | z+y | y | $C_o$-y |

Therefore, the equilibrium expression for $K_a$ from the values in Table 4.3 will be:

$$K_a = \frac{C_o - y}{(z+y)(y)} \qquad (9)$$

For our UV-Vis analysis to be correct, we need to know that y is sufficiently small compared to $C_o$. Assuming y is small compared to $C_o$ and to z, we can simply and solve for y according to the following relationship:

$$y = \frac{z}{K_a.C_\circ} \qquad (10)$$

This allows us to check that our approach would work by verifying that y is very small compared to $C_o$. Table 4.4 shows the results of this analysis, including the % value of y compared to $C_o$. As can be seen, the % value of y compared to $C_o$ is always less than 1%, verifying that our assumption was valid. In other words, the amount of $Zn^{2+}$ added was enough to ensure that the ZnL species were completely reformed in our UV-Vis studies.

**Table 4.4. The concentration values after adding an excess amount of $ZnCl_2$.**

| | z (M) | $C_\circ$(M) | x (M) | y | % |
|---|---|---|---|---|---|
| **Zn(L1)** | 0.010 | 0.0010 | $9.4\times10^{-6}$ | $8.5\times10^{-7}$ | 0.085 |
| **Zn(L2)** | 0.010 | 0.0010 | $2.0\times10^{-5}$ | $3.0\times10^{-6}$ | 0.30 |
| | 0.010 | 0.0020 | $7.3\times10^{-6}$ | $1.4\times10^{-7}$ | 0.0068 |
| | 0.010 | 0.0050 | $1.0\times10^{-4}$ | $4.8\times10^{-6}$ | 0.096 |
| | 0.010 | 0.50 | $2.5\times10^{-2}$ | $2.9\times10^{-5}$ | 0.0058 |
| **Zn(L4) +($Zncl_2$)** | 0.010 | 0.0020 | $8.0\times10^{-5}$ | $1.8\times10^{-5}$ | 0.88 |
| **Zn(L4) +$Zn(OAc)_2$** | 0.010 | 0.0020 | $2.3\times10^{-6}$ | $1.3\times10^{-8}$ | 0.00065 |

4.1.3. UV-Vis spectra of interactions between (ZnL) and inhibitors

In this section the interaction between (ZnL) and inhibitors were studied using UV-Vis spectroscopy. Because of the UV-Vis spectra of isolated (ZnL)-inhibitor structures are not known, the binding constants could not be obtained, but qualitative changes in the spectra were observed. In order to find $K_a$ values, the stoichiometry of the reaction with inhibitors as well as the molar absorbtivities of the ZnL-inibitor ternary complexes would be needed.

**Table 4.5. UV-Vis spectra of (ZnL) and inhibitors species.**

| Complex | ΔA | $C_o$ (mM) | Inhibitor (mg) | $\lambda_{max}$ (nm) |
|---|---|---|---|---|
| **Zn(L1)-SAHA** | 0.58 | 0.050 | 3.0 | 240 |
| **Zn(L1)-8HQ** | 2.4 | 0.050 | 7.0 | 308 |

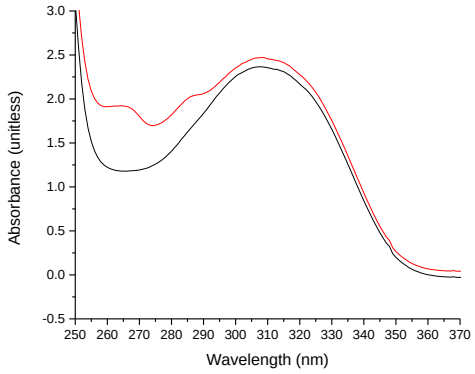


**Figure 4.4. UV-Vis spectra of Zn(L1)(8HQ) and 8HQ with the addition of Zn(L1)(8HQ) in ACN at a concentration of 0.050 mM.** The black spectrum represents 8HQ alone, and the $\lambda_{max}$ is 308 nm with an absorbance of 2.36. The addition of **Zn(L1)(8HQ)** (red), results in an increase in the spectra by 0.11 at the same wavelength, as well as the appearance of new peaks.

In order to examine the reaction of Zn(**L1**) for 8HQ, the UV-Vis spectra were taken for the 8HQ as well as a combination of Zn(**L1**) and 8HQ. In Figure 4.4, the black spectrum of shows a $\lambda_{max}$ of 308 nm and an absorbance value of 2.36. The spectrum of Zn(**L1**)(8HQ) was significantly different from that of just Zn(**L1**), indicating that we likely formed a complex between Zn(**L1**) and 8HQ. However, the identity of the species is unknown based solely on this

UV-Vis data and the NMR data in chapter 3. We hope that X-ray crystallography can be used in the future to determine the structure of the compound.

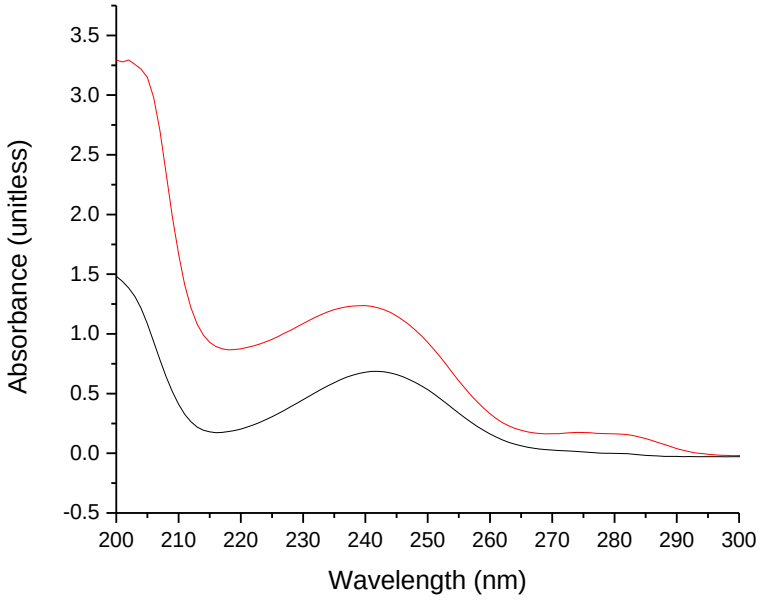


**Figure 4.5. The UV-Vis spectra of Zn(L1)(SAHA) (black) and with addition of SAHA (red) in ACN.** For the black spectrum, the $\lambda_{max}$ is 241 nm and the absorbance at $\lambda_{max}$ is 0.68. The addition of 8HQ (red), as 8HQ increases the spectra by 0.55 at the wavelength 240 nm.

Likewise, the interaction between Zn(**L1**) and SAHA was examined by using UV-Vis, at a concentration of 0.05 mM, the absorbance spectrum was obtained with a $\lambda_{max}$ = 241 nm. Upon addition of SAHA the absorbance at 241 nm was increased by 0.5. The association constant for this reaction could not be calculated due to the unknown stoichiometry of the resulting complex Zn(**L1**) and SAHA and the unknown molar absorptivity.

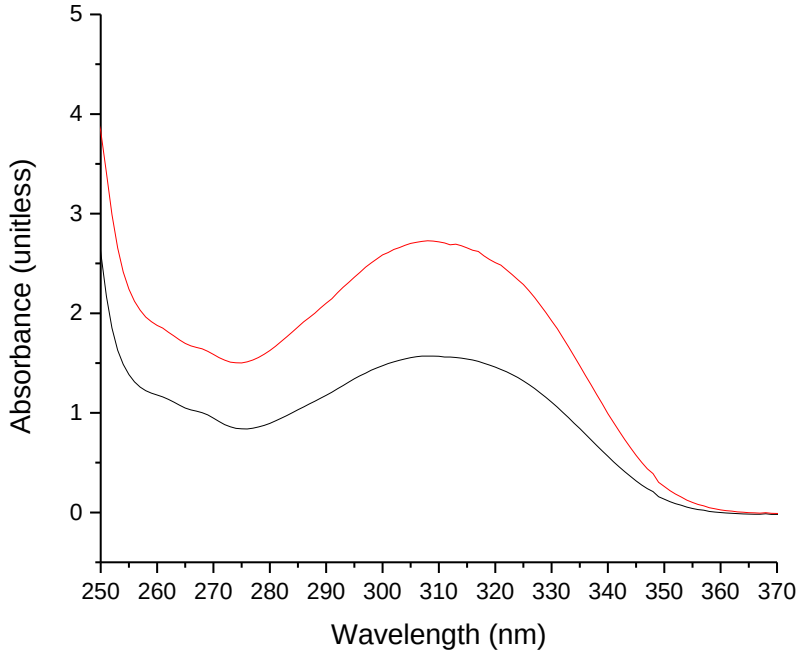


**Figure 4.6. UV-Vis spectra of Zn(L2) and 8HQ.** The spectrum in black indicates the absorbance of the Zn(L2) and 8HQ in concentration of 0.05 mM and the spectrum in red indicates the absorbance after the addition of 8HQ. For the black spectrum, the $\lambda_{max}$ is 307 nm and the absorbance at $\lambda_{max}$ is 1.57. The addition of 8HQ (red), as 8HQ increases the spectra by 1.15 at the wavelength 308 nm.

The interaction between Zn(**L2**)$Cl_2$ and 8HQ was studied using UV-Vis spectroscopy. The UV-Vis spectra show that the absorbance of the complex Zn(**L2**) and 8HQ was increased by 1.2 after adding a fixed amount of 8HQ (2.0 mg), but the data does not provide any insight into clear binding. Given the limited data that could be obtained from the UV-Vis studies of inhibitors reacting with the zinc complexes, we therefore turned to fluorescence spectroscopy.

4.2. Examining the binding of $Zn^{2+}$ with ligands and inhibitors by using fluorescence spectroscopy

4.2.1. Introduction

Fluorescence is defined as the emission of photons from an excited energy states as the system returns to a lower electronic state, such as in $S_1 \rightarrow S_0$ (Figure 4.7). If a certain species can absorb a specific energy of electromagnetic radiation, its electrons will be driven to a higher energy states (excitation). The absorbance as a function of wavelength yields an absorbance spectrum. However, these higher electronic energy states are unstable. Thus, the excited electrons will decay to their original lower energy states, which can result in the emission of light if they undergo a luminescence process. It should be noted that the wavelength of fluorescence emission should be higher than the absorbance wavelength, because the energy in the emission process is lower than in the absorbance process (some energy is always lost to relaxation processes that do not emit UV-Vis radiation).[31] In other words, the energy of the emitted light is always lower than the absorbing light because of the relationship between energy and wavelength:

$$E = \frac{hc}{\lambda} \qquad (9)$$

In which E is the photon energy, λ is the wavelength (nm), *h* is the Planck constant and c is the speed of light. Each photon released has its characteristic energy and it can be determined by subtracting the energy of the excited state and the energy of the ground state. Therefore, the gap between energy levels defines the photon energy. The fluorescence spectrometry for Zn-ligands is determined by the π – electrons of the conjugated organic ligand, because zinc does not have fluorescence character in the UV-Vis regions.[32] Fluorescence experiments were conducted to

study the interaction between 8HQ and SAHA with various ligand-$Zn^{2+}$ binary complexes that had been identified as potential HDAC functional mimetics based on the ligand and $Zn^{2+}$ ITC and UV-Vis studies. All complexes were dissolved in DMSO in very small amounts (sometimes the solution needed to be further diluted in order to detect the fluorescence emission signal on the scale of the spectrometry). Due to the small amounts used and the limits of accuracy on the balances, we did not determine the concentration of the solution. The data is presented without normalization, which may exaggerate the comparison of emission intensities. Because quantification was not possible, only qualitative changes in emission spectra were examined.

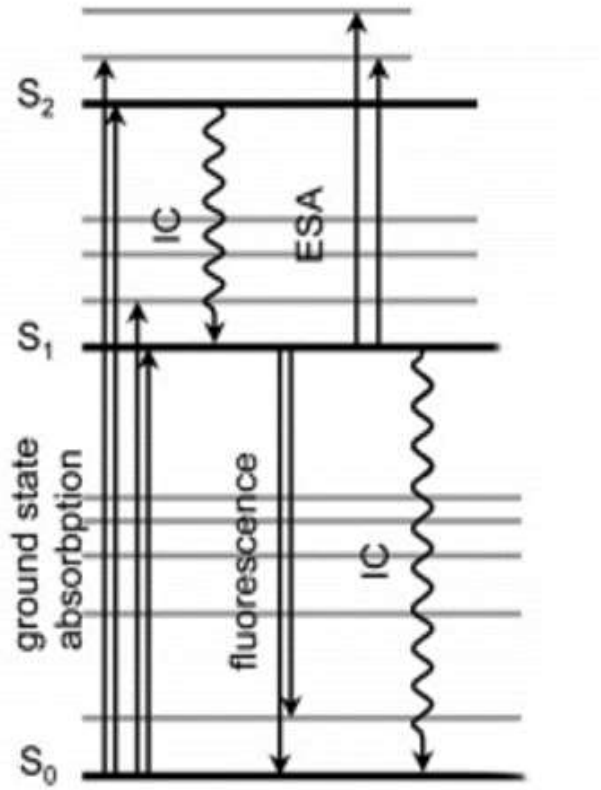


**Figure 4.7. Example Jablonski diagram for organic dyes**: IC—internal conversion, ESA—excited state absorption, ISC—intersystem crossing.[3]

4.2.2. Fluorescence spectra of Zn-ligand and inhibitor interactions

Three wavelengths were selected for fluorescence excitation: 240 nm, 260 nm, and 310 nm. The first two are excitations in the UV region where most of the compounds have absorption, and the 310 nm corresponds to absorption peaks in some of the Zn(L) complexes. These three values were kept consistent in order to make qualitative comparisons of the emission spectra. The fluorescence spectrum of the SAHA inhibitor was first obtained in order to compare with the zinc complexes (Figure 4.9). At an excitation 310 nm, a weak emission at $\lambda_{max}$ = 479 nm is observed (blue). Exciting at 240 nm yields no detectable emission. At an excitation of 260 nm, the spectrum displayed "negative emission", which is not an emission of SAHA, but rather likely noise. Both the positive and "negative" fluorescence intensities were very small.

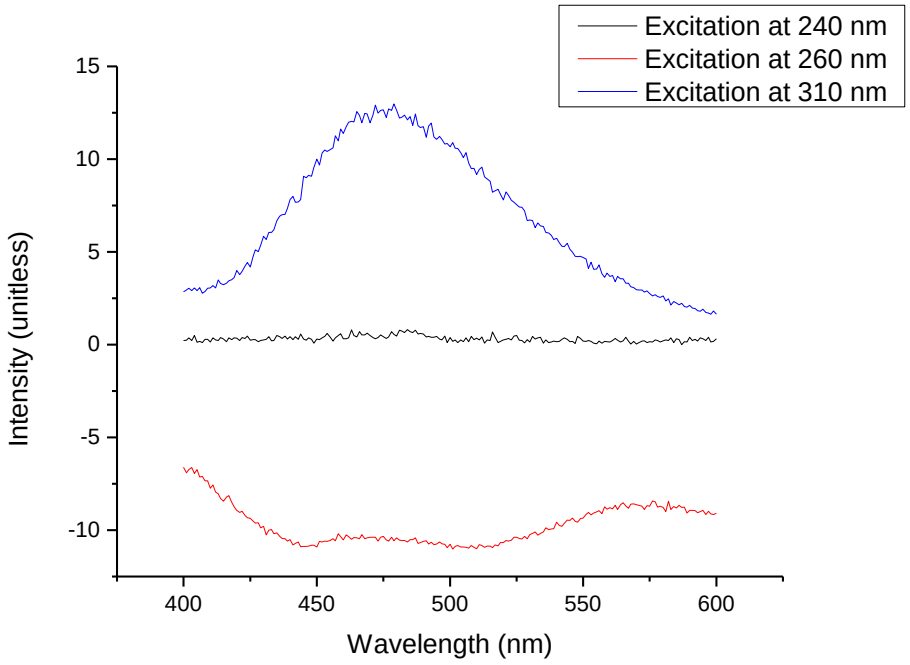


**Figure 4.8. The fluorescence emission wavelengths of free SAHA at excitation wavelengths 240, 260 and 310 nm.**

The fluorescence emission spectrum of Zn**(L1)** and SAHA was then recorded. The reaction was prepared by dissolving both compounds in DMSO. In the Figure 4.10, at excitation wavelength of 240 nm, the emission maximum was at 375 nm. The sharp peak observed at 484 nm is an artifact of the data collection. Often, sharp peaks are the harmonic of the excitation spectrum or other artifacts, and should not be considered to be emissions from the excited compounds. Exciting at 260 nm (not shown) resulted in no detectable emission. Exciting at 310 nm resulted in a sharp peak at 572 nm (likely an artifact) and a broad emission at 425 nm. The peak at 572 nm was observed as an unidentified artifact in several of our fluorescence spectra.

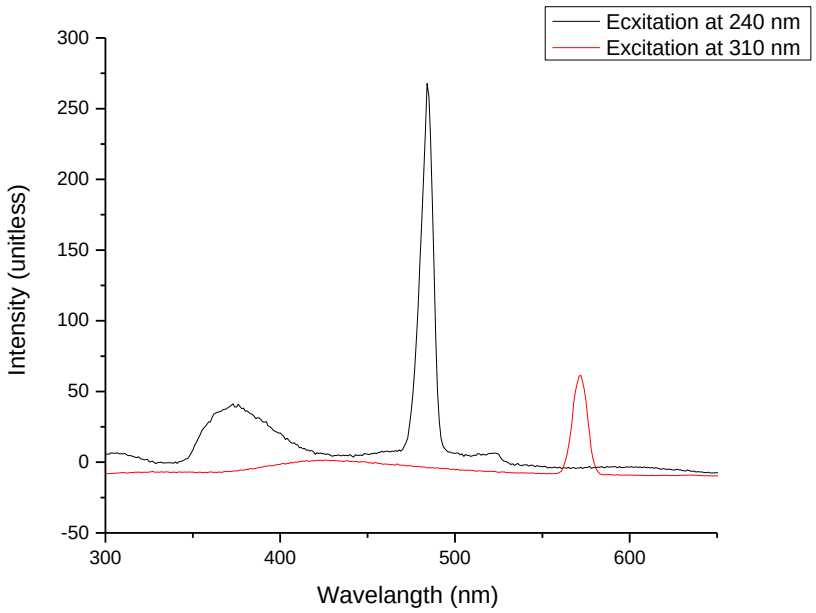


**Figure 4.9. The Fluorescence spectra of Zn(L1) and SAHA interaction**. The spectrum in red shows the emission in 310 nm, and the spectrum in black shows an emission with excitation at 240 nm.

The Fluorecsence spectra of Zn(**L2**), shown in Figure 4.11, showing one emission peak at 496 nm upon excitation at 240 nm. At 260 nm there was no observed emission, and at 310 nm three peaks were observed at 401 nm and 337 nm, as well as an artifact at 570 nm (Figure 4.10). When 8HQ was used as the inhibitor with Zn(**L2**) in DMSO, shown in Figure 4.12, emission peaks were observed at all 3 excitation wavelengths studied. At an excitation of 240 nm, only a small emission at 530 nm was observed. However, at 260 nm excitation, strong emission was observed at 492 nm. At 310 nm excitation, the emission at 492 nm moved to 482 nm, and small emission appeared at 344 nm as well. At excitation with 260 nm, Zn(**L2**) did not show emission. However, Zn(**L2**)(8HQ) shows two different emission peaks at higher wavelengths at this excitation. The fluorescence spectrum of free 8HQ (Figure 4.12) does not show the same peaks seen at all three excitations of Zn(**L2**) with 8HQ. Comparing emission of 8HQ and emission of Zn(**L2**)(8HQ), we can determine that there is some form of binding between Zn(**L2**) and 8-HQ based on the qualitative emission changes. In addition, these emission spectra were different from the emissions of just $Zn(8HQ)_2$ (Figure 4.15).

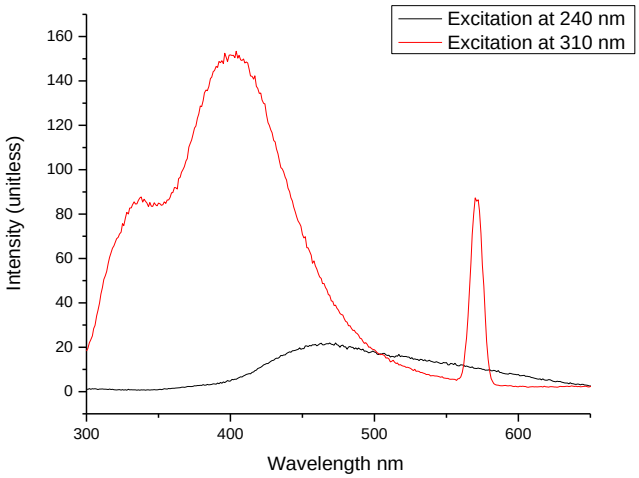


**Figure 4.10. The fluorescence emission of Zn(L2) at excitations of 240 nm and 310 nm.** An emission is observed at 400 nm upon excitation at 310 nm.

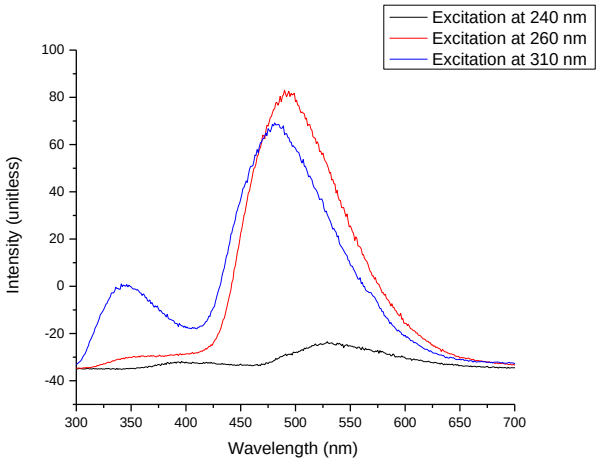


**Figure 4.11. The fluorescence spectra of Zn(L2) with 8HQ in DMSO**. Three emission spectra were observed after exciting the complex at excitations 240, 260 and 310 nm.

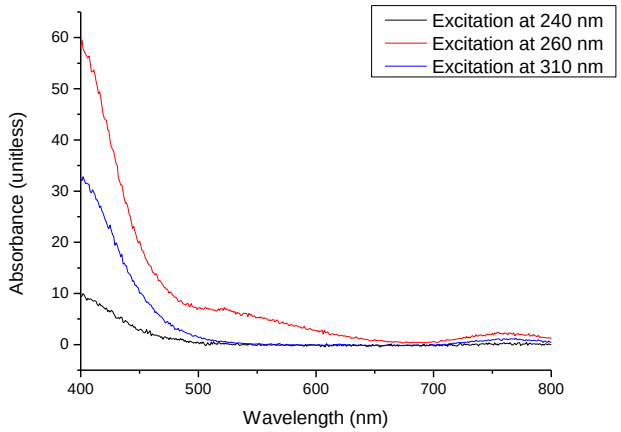


**Figure 4.12. Fluorescence spectra of 8HQ.** At excitation wavelengths 240, 260 and 310 nm. The product was dissolved in DMSO. An emission was observed at around 400 nm, but the spectral window examined did not allow for the peak wavelength to be observed.

When the isolated Zn(**L3**)OH species was studied in DMSO for fluorescence, the significant emissions were observed at 240 nm are a large  two peaks at 584 and 606 nm (likely a vibrational progression, Figure 4.14). At 260 nm excitation, an emission at 706 nm was observed. At 310 nm, only a likely harmonic artifact was observed.

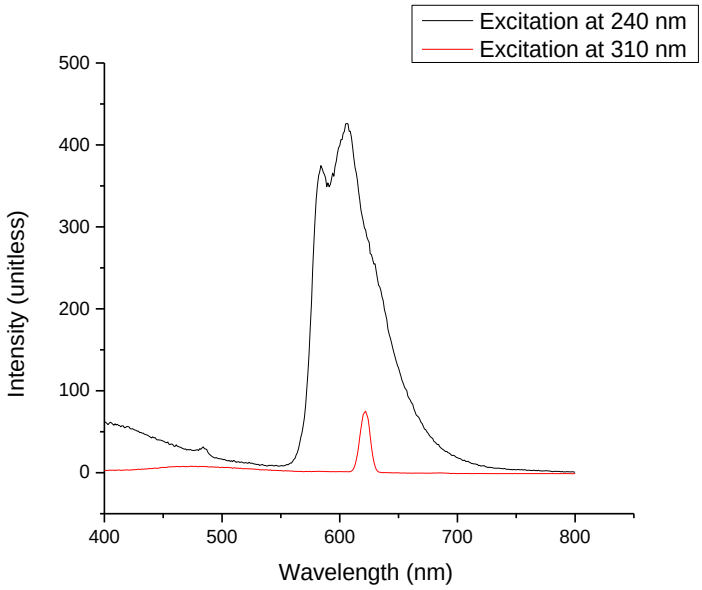


**Figure 4.13. Fluorescence emission of Zn(L3)OH in DMSO at excitations of 240 and 310 nm.** An emission was observed at around 400 nm at excitation 240 nm, but the spectral window examined did not allow for the peak wavelength to be observed. The peak observed at 622 nm is likely a harmonic of the excitation at 310 nm.

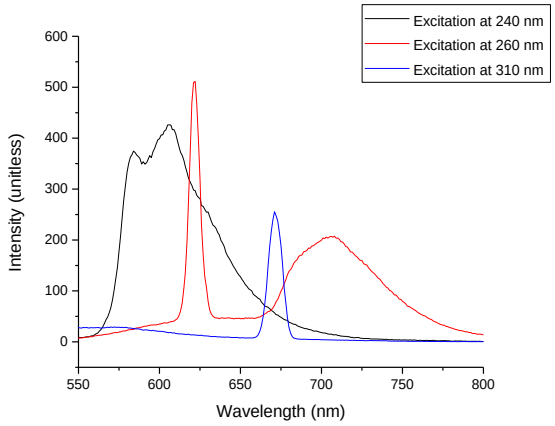


**Figure 4.14. The fluorescence spectra of Zn(L3)(8HQ) in DMSO.** Different emission behavior was observed after exciting the complex in 240, 260 and 310 nm.

The fluorescence spectra of Zn(**L3**(8HQ) show two major peaks at excitation 240 nm and one small peak at excitation wavelength 310 nm, along with the double harmonic of the excitation wavelength. In order to attempt to understand the spectra of Zn(**L3**)(8HQ), the known

$Zn(8HQ)_2$ species was studied with fluorescence. $Zn(8HQ)_2$ showed different behavior compared to Zn(**L3**)OH and Zn(**L3**)(8HQ) in that the same emission at 351 nm was observed at all 3 excitation wavelengths (Figure 4.15). Interestingly, at excitation with $\lambda = 260$ nm a new emission peak appeared at 543 nm as well.

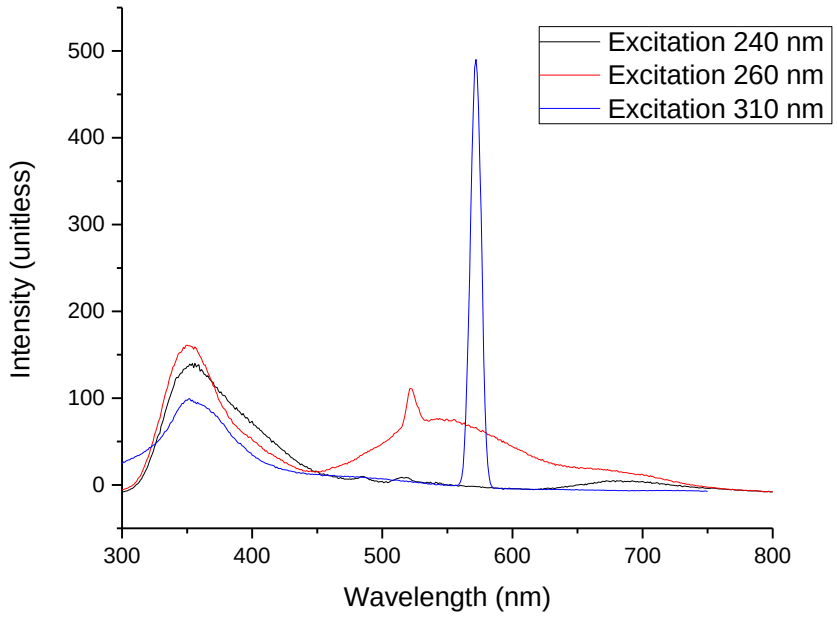


**Figure 4.15. Fluorescence spectra of $Zn(8HQ)_2$**. As shown the emissions of all excitations contain a feature at 351nm. There is also a clear broad peak at 543 nm upon excitation with 260 nm light. Other features are artifacts or harmonic peaks of the excitation wavelengths.

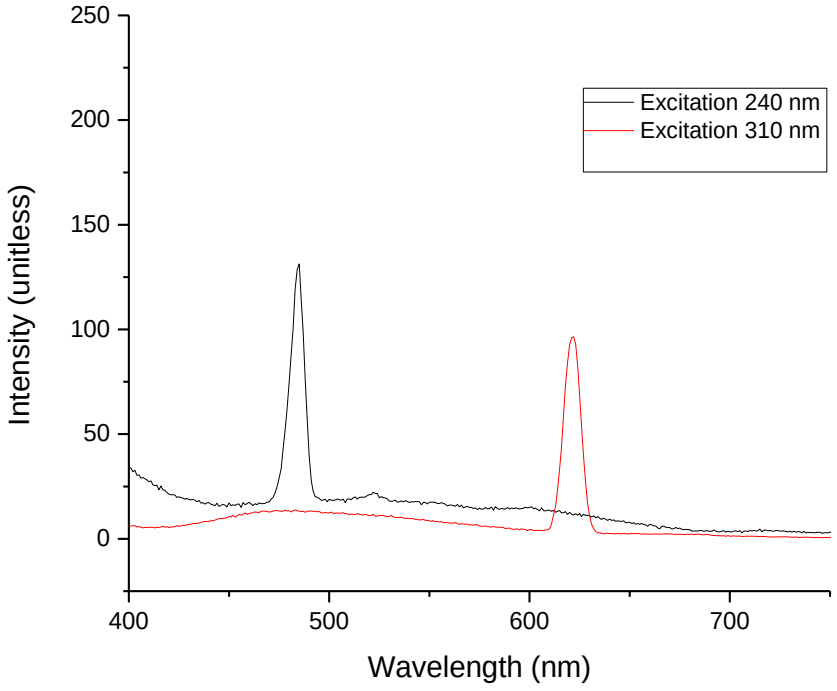


**Figure 4.16. Fluorescence spectra of $ZnCl_2$ and SAHA.** Both excitations studied did not result in significant emission signals (the sharp signals are artifacts).

The fluorescence spectra of the reaction mixture containing $ZnCl_2$ and SAHA were obtained at excitations 240 nm and 310 nm (Figure 4.16). Unfortunately, there were artifacts in the emission spectra but no clear major peaks.(similar to the fluorescence spectrum of SAHA). SAHA is inactive to fluorescence spectroscopy compared to 8HQ, which is likely due to the lack of conjugation in SAHA as compared to 8HQ.

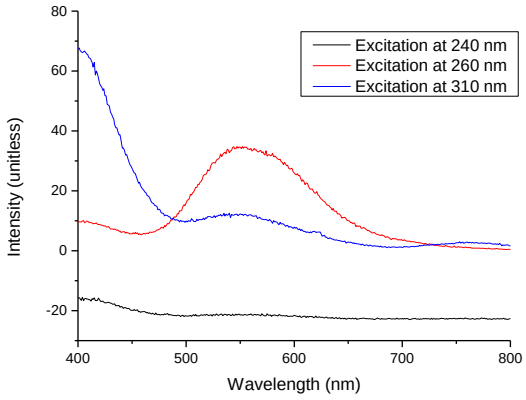


**Figure 4.17. The fluorescence spectra of Zn(L4) and 8HQ at excitation wavelengths 240, 260 and 310 nm.** A major feature at 550-560 nm is seen at excitations of 260 and 310 nm.

In Figure 4.18, the fluorescence spectra of Zn(**L4**) and 8HQ at all three excitation wavelengths is shown. At excitation with240 nm (black), the spectrum shows no major emission. However, at excitation with 260 nm, an emission peak was shown at wavelength 551 nm as well as a peak near 400 nm, and at excitation 310 nm, an emission shows at 555 nm wavelength. Comparing the fluorescence spectra of Zn(**L4**) and 8HQ with the fluorescence spectra of free 8HQ, there are clear differences, indicating that 8HQ can react with Zn(**L4**).

In conclusion, UV-Vis spectroscopy and fluorescence spectroscopy were used to study the zinc complexes and their interactions with inhibitors. UV-Vis spectroscopy of the (ZnL) compounds in the presence of added zinc was used to estimate $K_a$ values, which agreed reasonably well with ITC values in the case of BPA. However, the absorption values were high, and should be re-examined under more dilute conditions. Fluorescence was used to examine inhibitor interactions with zinc complexes, and 8HQ showed strong changes in responses when coordinated to zinc, whereas SAHA was found to not be very responsive to excitation in fluorescence spectroscopy. The fluorescence studies of the (ZnL) mimetic complexes and their

binding with inhibitors provide valuable information. We observed qualitative changes in the emission spectra of the various complexes in the presence of inhibitors, indicating that reactions were observed. Fluorescence of Zn(**L1**) and 8HQ showed emission spectra at 375 nm that was not observed with free 8HQ. When comparing the emission spectra of the reaction between Zn(**L2**) and 8HQ with the emission spectra of free 8HQ (Figure 4.12), the spectra also did not match. For the interaction between Zn(**L3**)OH with 8HQ (Figure 4.14), the emission spectra were different comparing to the emission spectra of free 8HQ or $Zn(8HQ)_2$ (Figure 4.15). Lastly, the Zn(**L4**) with 8HQ (Figure 4.17) show emission spectra that is also different than the fluorescence spectra of free 8HQ or $Zn(8HQ)_2$. We can conclude that Zn(L4) binds to 8HQ in solution and forms a product that is different than $Zn(8HQ)_2$. The data with SAHA were less conclusive because of the lack of significant fluorescence response from SAHA. Notably, quantitative studies of these and related complexes would be more informative, wherein the concentrations of all species are known and the extinction coefficients of the emission spectra can be determined. Further studies are also needed to understand the mechanism of the fluorescence from these compounds. Work toward these goals is ongoing in the Grice lab.

Bibliography**:**


1- Parkin, G., synthetic analogues relevent to the structure and function of zinc enzymes, *Chem. Rev.* **2004***, 104,* 699-767.

2- Rehder, D. Bioinorganic Chemistry *, Oxford University Press*. United Kingdom. **2014**. 152-153.

3- Silvernail. C.; Yao, L.; Hill, L.; Hllmyer, M.; Tolman,W. structural and mechanistic studies of bis(phenolato)amine zinc(ii) catalysts for the polymerization of ε-caprolactone. *Inorg Chem* **2007,** 46, 6565–6574.

4- McCal, K.; Huang, C.; Fierke, C., function and mechanism of zinc metalloenzymes. *The Journal of nutrition* **2000**, 130 (5S Suppl), 1437S-46S.

5- Claudiu. S, Carbonic anhydrases: novel therapeutic applications for inhibitors and activators. *General Review*. **2008**, *7*, 168-181.

6- Vallee, B.; Auld, D., zinc: biological functions and coordination motifs. *Acc. Chem. Res* ***1*993**, 26, 543–551.

7- Gupta, S. Hydroxamic acids a unique family of chemicals with multiple biological Activities. *Springer Berlin Heidelberg*. India. **2013**, 11-12

8- Cohen, Joshua A. Day and Seth M. Investigating the Selectivity of Metalloenzyme Inhibitors. *Med. Chem*. **2013**, *56 (20),* 7997–8007

9- Song, Y. X.; Chen, W.; Zhan, P.; Liu, X., 8-hydroxyquinoline: a privileged structure with a broad-raning pharmacological potential, *Med. Chem. Commun.* **2015,** *6*, 61-74

10- Miller, T.; Witter, D.; Belvedere, S., Histone deacetylase inhibitors. *J. Med. Chem* **2003***, 46,* 24, 5097–5116.

11- Kouzarides, T. chromatin modifications and their function. *Cell.* **2007***,128,* 693–705.

12- Witt, O.; Deubze, H.; Milde, T.; Oehme, I., HDAC family: what are the cancer relevant targets?, *Cancer Letters* **2009***, 277,* 8-21.

13- Sun Cao, P.; Sommer, R.; Grice, K., structural comparison of suberanilohydroxamic acid (SAHA) and other. *Polyhedron. **2016**, 116,* 344–350.

14- Finnin, M.; Doniglan, J.; Cohen, A.; Richon, V.; Rifkind, R.; Marks, P.; Breslows,R.; Paveletich, N., Structures of a histone deacetylase homologue bound to the TSA and SAHA inhibitors. *Nature* **1999**, 40, 188-193.

15- Griffitha, D.; Szocs, B.; Keogh, T.; Suponitsky, K.; Farkas, E.; Buglyó, P. Suberoylanilide hydroxamic acid, a potent histone deacetylase inhibitor; its x-ray crystal structure and solid state and solution studies of its Zn(ii), Ni(ii), Cu(ii) and Fe(iii) complexes. *Journal of Inorganic Biochemistry.* **2011**, 105(6), 763–769.

16- Robinson, S. Burns, P. Miceli, A. Grice, K. Karver, C. Jin, L. Calorimetric studies of the interactions of metalloenzyme active site mimetics with zinc-binding inhibitors. *Dalton Trans.* **2016**, *45,* 11817.

17- Wirbser, J. Vahernkamp, H. Zinc Complexes of Cain-Like $N_3$ Chelate Ligands. *Journal of Chemical and Sciences*. **1992**, *7,* 962-968.

18- Barroso, S. Abreu, A. Araujo, A. Coelho, A. Maulide, N. Martins, A. Three-Component Mannich Coupling En Route to Substituted Aminophenol and Benzoxazine Derivative. *Synlett*. **2010**. 16, 2425-2428

19- Greenberg, A. Breneman, C. Liebman, J. The amide linkage, Structural significance in chemistry, biochemistry and materials science. *Ajohn Wiley and Sons, Inc. Publication*. USA. **2000**, *3*, 47-50

20- Liana Hie, Noah F. Fine Nathel, Tejas K. Shah, Emma L. Baker, Xin Hong, Yun-Fang Yang,Peng Liu, K. N. Houk & Neil K. Garg. Conversion of amides to esters by the nickel-catalysed activation of amide C–N bonds. *Nature letter.* **2015***,* 524, 79–83.

21- Ouyang, K. Wei Hao. Wen-Xiong Zhang. Zhenfeng Xi. Transition-Metal-Catalyzed Cleavage of C−N Single Bonds.(2015). Chem. Rev. **2015**, 115, 12045−12090.

22- Greenberg, A.; Curt M.; Breneman, J.; Liebman, F. The Amide Linkage: Structural Significance in Chemistry, Biochemistry, and Materials Science. *John Wiley and Sons*. New York. **2000**, *4*, 85- 90.

23- Chen, K.; Liping, X.; Wiest, O., Computational exploration of zinc binding group gor hdac inhibition*, J. Org, Chem.* **2013***, 78*, 5051- 5055.

24- Day, J.A. Cohen, S.M. Investigation the selectivity of metalloenzyme inhibitors. *J. med. chem.* **2013**, 56, 7997, 8007.

25- Dokmanovic, M. C., C.; Marks, P.A.*,* Histone Deacetylase Inhibitors: Overview and Perspectives. *Mol. Cancer. Res.* **2007,** 5 (10), 981-989.

26- Falkenberg, K. J. J., R.W., Histone deacetylases and their inhibitors in cancer, neurological diseases and immune disorders. *Nature Reviews.* **2014**, 13, 673-691.

27- Frisch, M. J. T., G. W.; Schlegel, H. B.; Scuseria, G. E.; Robb, M. A.; Cheeseman, J. R.; Scalmani, G.; Barone, V.; Mennucci, B.; Petersson, G. A.; Nakatsuji, H.; Caricato, M.; Li, X.; Hratchian, H. P.; Izmaylov, A. F.; Bloino, J.; Zheng, G.; Sonnenberg, J. L.; Hada, M.; Ehara, M.; Toyota, K.; Fukuda, R.; Hasegawa, J.; Ishida, M.; Nakajima, T.; Honda, Y.; Kitao, O.; Nakai, H.; Vreven, T.; Montgomery, J. A., Jr.; Peralta, J. E.; Ogliaro, F.; Bearpark, M.; Heyd, J. J.; Brothers, E.; Kudin, K. N.; Staroverov, V. N.; Kobayashi, R.; Normand, J.; Raghavachari, K.; Rendell, A.; Burant, J. C.; Iyengar, S. S.; Tomasi, J.; Cossi, M.; Rega, N.; Millam, J. M.; Klene, M.; Knox, J. E.; Cross, J. B.; Bakken, V.; Adamo, C.; Jaramillo, J.; Gomperts, R.; Stratmann, R. E.; Yazyev, O.; Austin, A. J.; Cammi, R.; Pomelli, C.; Ochterski, J. W.; Martin, R. L.; Morokuma, K.; Zakrzewski, V. G.; Voth, G. A.; Salvador, P.; Dannenberg, J. J.; Dapprich, S.; Daniels, A. D.; Farkas, Ö.; Foresman, J. B.; Ortiz, J. V.; Cioslowski, J.; Fox, D. J. Gaussian 09, Gaussian, Inc.: Wallingford, CT, **2009**.

28- Foresman, B. J., Frisch, A. Exploring chemistry with electronic structure methods. Second Edition. Gaussian, Inc. USA. **1996**.

29- Codd, R. Traversing the coordination chemistry and chemical biology of hydroxamic acids. *Coordination Chemistry Review*, **2007,** 1387–1408.

30- Thordarson, P. Determining association constants from titration experiments in supramolecular chemistry. *Tutorial Review*. **2010**. *40,* 1305-1323

31- Valeurn, P. Berberan-Santos, M. Molecular Fluorescence: Principal and applications, 2nd addition. **2012**. Chapter 3.

32- Valeurn, P. Berberan-Santos, M. Molecular Fluorescence: Principal and applications, 2nd addition. **2012**. Chapter 4, 22.

Figure Sources:


1- Vullo, D. Supuran, C. T. Scozzafava, A. De Simone, G. Monti, S.M. Alterio, V. Carta, F. kinetic and x-ray crystallographic investigation of substituted 2-thio-6-oxo-1,6-dihydropyrimidine-benzenesulfonamides acting as carbonic anhydrase inhibitors. *Bio org Med Chem.* **2016.** 24.

2- ubert, S. Biochemistry. Biochemistry. 4th; *W. H. Freeman and Company.* New York – Basingstoke,**1995**.

3- Zimmermann, J.; Zeug, A.; Roder, B. A generalization of the Jablonski diagram to account for polarization and anisotropy effects in time-resolved experiments. *Phys. Chem*. **2003**, *5*, 2964–2969.